

# Two-colour fluorescence-based method for detecting virus particles in solution

Master's thesis in Applied Physics

FRIDA ULANDER



MASTER'S THESIS 2016

**Two-colour fluorescence-based method for  
detecting virus particles in solution**

FRIDA ULANDER



**CHALMERS**  
UNIVERSITY OF TECHNOLOGY

Department of Physics  
*Division of Biological Physics*  
CHALMERS UNIVERSITY OF TECHNOLOGY  
Göteborg, Sweden 2016

Two-colour fluorescence-based method for detecting virus particles in solution  
FRIDA ULANDER

© FRIDA ULANDER, 2016.

Supervisor: Olov Wahlsten, Department of Physics  
Examiner: Fredrik Höök, Department of Physics

Master's Thesis 2016  
Department of Physics  
Division of Biological Physics  
Chalmers University of Technology  
SE-412 96 Göteborg  
Telephone +46 31 772 1000

Cover: Two sets of coloured vesicles attaching to virus-like particles and being excited by dual-colour laser.

Printed by Reproservice  
Göteborg, Sweden 2016

# Two-colour fluorescence-based method for detecting virus particles in solution

FRIDA ULANDER

Department of Physics

Division of Biological Physics

Chalmers University of Technology

Göteborg, Sweden 2016

## Abstract

In our globalized world people travel all over the planet in work and for leisure. But with the intensified travelling comes the effect of diseases spreading fast between continents. In case of outbreaks or epidemics, impeding spreading of diseases is of great importance and there is thus a great need of fast, reliable and sensitive virus detection methods. User-friendly detection methods could be placed at for example airports to identify virus carriers.

In this thesis a novel method for detecting small amounts of viruses in solution is evaluated. The assay is based on fluorescence microscopy and by having fluorescently labelled biological molecular assemblies, called vesicles, in a solution. The role of the vesicles is to act as reporters for the unlabelled virus particles. When adding a sample containing viruses, the vesicles and viruses interact specifically, bind to each other and form complexes. By recording the movement of the vesicles with a microscope the vesicles can be tracked individually by a software. Half of the vesicles are labelled so that they are being excited by a red laser and half of the vesicles so that they are excited by a blue laser. The two subpopulations are tracked separately in the microscope. By finding events where a red and a blue particle are moving correlated, the viruses can be detected since a blue and a red particle moving together indicates that they are held together by a virus.

The lowest virus concentrations to be detected was 10 pM by tracking particles and detecting colocalization events. By analysing the same data with an alternative method based on overlaying images instead of single-particle tracking, the processing time was significantly reduced, still with a limit of detection of 10 pM. However, for both analysis methods, the contrast between samples with high virus concentration and samples with no viruses was only on the order of 4. This can be partly due to limitations in the data analysis and also to the vesicles interacting unspecifically with each other.

**Keywords:** colocalization, dual-colour microscopy, virus detection, single-particle tracking, SV40.



## Acknowledgements

This thesis would not have seen the light of the day if were it not for a lot of people who have helped and supported me during the process. I have learned so much during the last months, and it is because of you all. Thank you!

**Olov Wahlsten**, the best supervisor I could have wished for. Thank you for your enthusiasm and for trying to teach me everything you know. And for your music tips.

My examiner **Fredrik Höök** for valuable comments and especially for introducing me to the world of biological physics.

**The Biological Physics group** for lunches, fikas and after works. For all the laughs during the weird discussions at the fika room.

**Stephan Block** for always answering my questions, regardless of how much you have to do.

**Björn Agnarsson** for helping me out with the microscope.

**Friends** at Engineering Physics, for making these five years much more pleasant. I am starting to feel very nostalgic about the time here.

**Oscar**, for your patience, support and ideas. You mean everything to me.

Frida Ulander, Göteborg, June 2016



# Contents

<b>List of abbreviations</b>	<b>vi</b>
<b>1 Introduction</b>	<b>1</b>
1.1 Outline . . . . .	2
<b>2 Biological foundation</b>	<b>3</b>
2.1 Lipid bilayers and vesicles . . . . .	3
2.2 Simian virus 40 . . . . .	4
2.3 Ganglioside GM1 . . . . .	6
2.4 Cholera toxin . . . . .	6
<b>3 Virus detection</b>	<b>9</b>
3.1 Traditional and modern virus detection methods . . . . .	9
3.2 Idea of colocalization assay with dual-colour fluorescence microscopy	11
3.2.1 Past studies with dual-colour microscopy colocalization . . . .	11
<b>4 Theoretical aspects</b>	<b>13</b>
4.1 Collision frequency in solution . . . . .	13
4.2 Diffusion of aggregates . . . . .	15
4.3 Theoretical limit of detection . . . . .	16
<b>5 Materials and methods</b>	<b>17</b>
5.1 Preparation of vesicles . . . . .	17
5.1.1 Determination of excitation and emission spectrum for fluo- rophores . . . . .	18
5.2 Quartz-crystal microbalance with dissipation monitoring . . . . .	18
5.3 Nanoparticle tracking analysis . . . . .	19
5.4 Colocalization assay . . . . .	21
5.4.1 Choice of objective . . . . .	22
5.5 Data analysis . . . . .	24
5.5.1 Aberration correction . . . . .	26
<b>6 Results</b>	<b>29</b>
6.1 Verification of vesicles-virus interaction . . . . .	29
6.2 Vesicle size distribution and aggregation . . . . .	30
6.3 Excitation and emission spectrum for fluorophores . . . . .	32

6.4	Experiments with colocalization assay . . . . .	33
6.4.1	Performance test for colocalization assay . . . . .	33
6.4.2	Limit of detection . . . . .	35
6.4.2.1	Dependence on incubation time . . . . .	37
6.4.2.2	Choice of analysis criteria . . . . .	38
6.4.2.3	Alternative analysis . . . . .	40
<b>7</b>	<b>Discussion</b>	<b>43</b>
7.1	Limitations in colocalization assay . . . . .	43
7.1.1	Upper limit of virus concentration . . . . .	43
7.1.2	Interrupted tracks . . . . .	44
7.1.2.1	Setup modification . . . . .	44
7.1.3	Unspecific interactions . . . . .	45
7.1.4	Problem with out-of-focus vesicles . . . . .	46
7.2	Comparison between NTA and colocalization assay . . . . .	48
<b>8</b>	<b>Conclusion</b>	<b>49</b>
<b>9</b>	<b>Future outlook</b>	<b>51</b>
	<b>Bibliography</b>	<b>53</b>

# List of abbreviations

<b>CTB</b>	Cholera toxin B
<b>DOPE</b>	1,2-dioleoyl-sn-glycero-3-phosphoethanolamine
<b>GM1</b>	monosialotetrahexosylganglioside
<b>NTA</b>	Nanoparticle tracking analysis
<b>PBS</b>	Phosphate buffered saline
<b>POPC</b>	1-palmitoyl-2-oleoyl-sn-glycero-3-phosphocholine
<b>QCM-D</b>	Quartz-crystal microbalance with dissipation monitoring
<b>SV40</b>	Simian virus 40
<b>VLP</b>	Virus-like particle



# 1

## Introduction

THE TRANSITION from a lifestyle of hunting and gathering to one of agriculture and settlement marked a major turning point in the human history. Domesticating plants and animals meant that larger groups of people could be supported, laying the foundation to grand societies. However, a new threat emerged as the human population grew, in form of virus specialized in humans [1, 2]. Several diseases originally infecting animals started to spread from animal to human, and eventually from human to human. Since the Neolithic revolution 10 000 years ago waves of epidemics have effectively reduced the human population and occasionally changed the course of history.

As a process of natural selection, many people develop resistance when exposed to a virus. However, exposing a group to a virus new to them can have dire consequences. When Cortés came to Mexico in 1519 with only 600 soldiers, they were able to conquer the Aztec Empire despite being outnumbered by millions of Aztecs. The Spanish conquistadors were better equipped with weapons, but this in itself had probably not been enough to overthrow a whole empire. Nevertheless, when half of the Aztec population succumbed to smallpox introduced in 1520 this eased the process for the Spanish considerably [3].

Diseases can only spread as fast as their carriers and when transportation was slow, proliferation was slow. A journey to another country or continent could take months, or even years, when transportation was limited to horse-riding, going by boat or walking. Occasional travellers was enough for starting an outbreak, but many people never travelled farther than to the next village. The last 200 years, the mobility of people have increased dramatically with the introduction of railroad and aviation. The society has become more and more globalized, and it is now not only possible to travel to the other side of the world in twelve hours, it is also rather common to do this in work or for leisure. This means that viral diseases also can spread across the world in the same time. With incubation times for virus infections typically varying from a couple of days to a couple of weeks, there is a possibility of people travelling unaware of being ill and of spreading a disease [4, 5]. A carrier coming in contact with potentially non-exposed people can cause rapid spreading with high infectious rates. One example is the Zika virus, spreading from Africa to Brazil the last years, where it is believed to cause birth defects [6, 7]. It is thus of great importance of having fast and reliable methods for virus detection at for example

airports for minimizing proliferation of dangerous diseases between countries and continents.

In this thesis, a novel method for detecting low levels of viral particles based on fluorescence microscopy is investigated with regards to limit of detection and time limitations. The technique is based on having fluorescent particles mixed with virus particles in a solution. The fluorescent particles, marked with recognition elements, interact specifically with the viruses which cause the fluorescent particles to form complexes. The viruses are identified by finding such complexes by individual tracking of the fluorescent particles. The purpose is to determine the limit of detection and the time scale of detection. One key question to address is whether it would be possible to use this method for virus detection at an airport, with an hour between security and boarding.

## 1.1 Outline

The structure of the thesis is outlined below. The first chapters includes an introduction to biological molecules and the methods used in the thesis. Then follows experimental results and some theoretical aspects with the last chapters discussing the results in a larger perspective.

- **Chapter 2 - Biological foundation** For those not familiar with biological physics, this chapter gives a short introduction to important biological molecules and other molecules used in the experimental parts of this thesis.
- **Chapter 3 - Virus detection** This chapter gives a brief introduction to existing conventional virus detection methods and their advantages and limitations.
- **Chapter 4 - Methods** A summary of the technologies and instruments used in the project is covered in this chapter.
- **Chapter 5 - Theoretical aspects** In this chapter some thoughts about the theoretical aspects of the system is presented, such as the theoretical limit of detection.
- **Chapter 6 - Results** The main experimental results are summarized here.
- **Chapter 7 - Discussion** In this chapter the results are discussed further in terms of limitations.
- **Chapter 8 - Conclusion** The main findings are summarized here, to give an overview of what was achieved in the project.
- **Chapter 9 - Future outlook** A couple of suggestions to how the project could be further developed is given in this chapter.

# 2

## Biological foundation

FOR THOSE not entirely familiar with biology or biological physics, this chapter provides an introduction to fundamental biological structures, focusing on the molecules and particles used in the experimental parts of this thesis.

### 2.1 Lipid bilayers and vesicles

Lipids belong to one of the four classes of biological macromolecules that are the fundamental building blocks for all living organisms, the other being proteins, carbohydrates and nucleic acids. They all consist of mostly carbon, oxygen, nitrogen, sulphur and phosphorus, however, they show a tremendous diversity in form of structure and serve very different purposes. Proteins form structural elements in cells and catalyses important reactions. Carbohydrates are responsible for energy storage and may also form more rigid structural elements outside the cell. Nucleic acids store genetic material enabling cells to replicate. Lipids form cell membranes, separating the interior of the cell from the surrounding world. Together they are the foundation of living structures [8].

Lipids are partly hydrophobic, partly hydrophilic molecules making up the cell membrane. With *hydro* meaning water, *phobia* meaning fear and *philia* meaning love in Greek, lipids have one part that will avoid water and one that embraces it. The diversity among lipids is large but a common characteristic is the existence of a hydrophilic head group and one (or more) hydrophobic tails (usually fatty acids). Lipids vary in size, number of tails and molecular composition of head group and tails. In a solution with many lipids, the head groups screen the tails from the aqueous surrounding, causing the lipids to form aggregates. One common form is the *bilayer*, where the lipids arrange into two layers with the heads making up the surface and the tails pointing inwards. To avoid edge effects closed structures, such as spherical shells, or *vesicles* are often formed. Figure 2.1 depicts schematically a lipid, a vesicle in an aqueous solution and a part of a bilayer formed on a solid support. The bilayer (and thus the vesicle) can be seen as a two-dimensional fluid where individual lipid molecules will diffuse around. The bilayer, and the vesicle, can also bend, stretch and change shape.

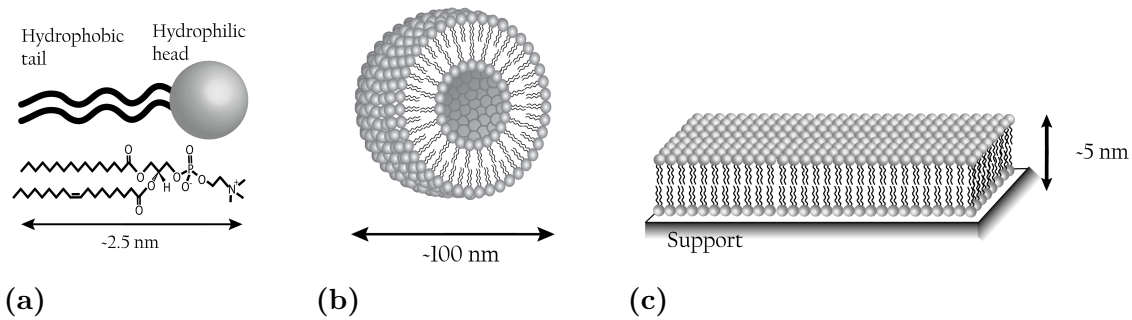


**Figure 2.1:** An illustration of a) a lipid, b) a vesicle and c) a lipid bilayer formed on a solid support.

The bilayer membrane in cells constitutes of many different lipids and membrane proteins [8]. A lipid often used in biophysical experiments is 1-palmitoyl-2-oleoyl-sn-glycero-3-phosphocholine, abbreviated *POPC* [9]. *POPC* is a synthetic mimic of the most abundant lipid in mammalian cells [8]. The lipids self-assemble into vesicles in solution [10] and it is possible to customize the vesicles by adding for example receptors or membrane proteins. In the experiments in this thesis, *POPC* is the main constituent of the vesicles. Another lipid used in experiments in this thesis is 1,2-dioleoyl-sn-glycero-3-phosphoethanolamine, abbreviated *DOPE*, which is used as a carrier for fluorophores to label the vesicles.

## 2.2 Simian virus 40

A virus is a biological entity that infects and replicates inside host cells [8]. They exist in all parts of ecosystems; some infecting animals or plants; others specializing in bacteria or other microorganisms. Viruses exhibit a great diversity, regarding for example protein content, genetic content, structure and effect on the host [11]. For example, the effect of human infecting viruses range from a common cold to AIDS and Ebola. There are millions of kinds of viruses, still only a fraction of them being studied thoroughly [12].

The variety among viruses is large, but some characteristics can be distinguished. The outer part of a virus usually consists of a shell of proteins, assembled into a symmetric structure called a *capsid* [8]. Within the capsid the genetic material is stored. The genetic material can be single-stranded or double-stranded DNA or RNA. Some viruses also have a lipid membrane covering the protein shell, called enveloped viruses. Viruses lacking this membrane are called non-enveloped. The size ranges from tens to hundreds of nanometres and their shape can be sphere-like, rod-like or more complex.

In this thesis a virus called Simian Virus 40, abbreviated *SV40*, is being detected. Named after the simian monkey, it is a non-enveloped DNA virus whose natural host is Asian macaque monkeys [13]. It has been shown to cause tumours, however,

it is most often latent [13]. SV40 was discovered during the development of the polio vaccine, when it was found to be contaminating the early forms of the vaccine [14].

Being approximately 40 nm in diameter, SV40 is quite small compared to other viruses and has a protein shell encapsulating the genetic material [13, 15]. The protein shell, the capsid, consists of 360 copies of the structural protein VP1, ordered in 72 pentamers [16], illustrated in Figure 2.2. VP1 is the protein involved in attachment to cells [17]. Each VP1 monomer folds into a pleated sheet and assembles with four others. "Arms" stretch out from the pentamers, interacting with other pentamers and holding the structure together. The pentamers assemble into a icosahedron containing two other proteins; VP2 and VP3.

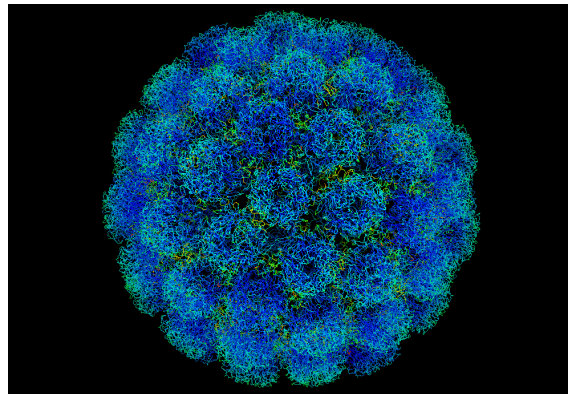


**Figure 2.2:** An illustration of SV40, with the capsid consisting of 360 copies of the protein VP1. Each blue ring is a pentamer with 5 VP1 proteins. The green parts are "arms" that hold the structure together. The proteins VP2 and VP3 are not visible in the figure. Picture source: Wikimedia Commons [18].

While infecting, SV40 attaches to cells and the receptor involved in endocytosis is the ganglioside GM1 [15, 17], a molecule that will be briefed in the next section. SV40 interacts with this molecule with high specificity [16], thus not binding to many other proteins. When attaching to a cell, SV40 can attach to several GM1 proteins, yielding a high affinity due to multivalent binding [15]. This induces a curvature of the membrane, enabling endocytosis [15].

A *virus-like particle* (VLP) is a virus with no genetic material, most commonly produced by self-assembly of proteins produced in for example bacteria or insect cells [19]. With no genetic material, the virus cannot reproduce and is thus non-infective and safe to work with. When studying only the interaction of the virus and not the endocytosis or replication, using virus-like particles is a simple way to reduce/remove the risks during experiments [19]. In this thesis, virus-like particles of SV40 have been used instead of live SV40.

## 2.3 Ganglioside GM1

A ganglioside is a type of glycosphingolipid appearing in neural cells in the brain, consisting of a number of carbohydrates and a ceramide tail with a number of sialic acids attached [20]. The abundance in neural cells (up to 10 % of total lipid content) indicates a prominent role in the nervous system [20]. They are also associated with neural diseases and possible therapeutical applications is therefore investigated [20].

There are several types of gangliosides, classified by the combination of sugars and number of sialic acids. The chemical structure of GM1 is shown in figure 2.3. GM1 consists of four carbohydrates and one sialic acid with a ceramide tail [16]. The overall structure resembles the letter "Y" where the tail is embedded in the membrane. Both branches of the "Y" is in contact with SV40 during attachment [20, 16].

Gangliosides, including GM1, can be purchased commercially for experimental use. Dissolving gangliosides with lipids result in GM1 being incorporated into the bilayer when the lipids self-assemble into vesicles.

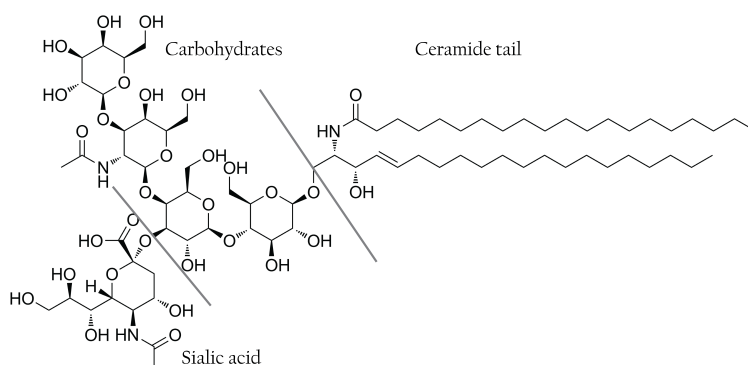


**Figure 2.3:** Chemical structure of GM1, consisting of four carbohydrates, one sialic acid and a ceramide tail.

## 2.4 Cholera toxin

Cholera toxin is a toxic substance produced by the bacteria *Vibrio cholerae* which causes the, sometimes severe, disease cholera. It has been shown that cholera toxin can enter cells in a similar way as SV40; by attaching to GM1 receptors in the cell membrane [16]. Cholera toxin has a pentameric structure with one "A" subunit and five "B" subunits which can thus attach to five GM1 molecules. Figure 2.4 illustrates the configuration of A and B subunits. Cholera toxin has a very high affinity towards GM1 - much higher than SV40 - and will compete out SV40 or other molecules attaching to GM1 [16, 21]. This effect makes it suitable as an inhibitor for the reaction SV40-GM1 or other interactions involving gangliosides.

Removing the toxicity-controlling "A" subunit yields the non-toxic cholera toxin B, abbreviated CTB, suitable for experiments [22].

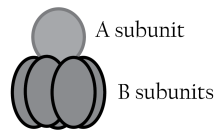


**Figure 2.4:** *Illustration of cholera toxin. The top part is the toxic subunit A, and the other five identical parts are the B-subunits. Removing the top part yields cholera toxin B, which is used in this thesis.*



# 3

## Virus detection

THE POTENTIAL DANGERS of viral diseases emphasize the need of fast and sensitive methods for detecting virus. Due to the great diversity among viruses, there is not yet one universal detection method. The most commonly used methods for virus detection can roughly be divided into three categories: techniques for measuring viral infectivity, techniques for examining viral nucleic acids and proteins and methods for directly counting viral particles. In the following sections, a couple of methods will be briefly enlightened in order to give an introduction to virus detection and to account for the challenges still existing. The chapter is not meant to be a profound review of all existing methods, but rather to give the reader an introduction to virus detection and to point out the diversity of methods. In the last section, the main ideas of the assay used in this thesis are introduced, the so-called colocalization assay.

### 3.1 Traditional and modern virus detection methods

The earliest method developed for counting viral particles was the *plaque assay* in 1917, still widely used today in different variations [23, 24]. With this method, the number of infectious particles is counted via the formation of so called *plaques*. To produce the plaques, a virus stock is added to a susceptible cell monolayer, covered by a semi-solid medium such as agar. As the viruses infect neighbouring cells, infectious particles produces a circular zone of infected cells - a plaque [25]. This can take 3 to 14 days depending on virus type. The plaques can then be imaged with a microscope, and eventually visible by naked eye. This method is applicable only for viruses that cause visible damage to the cells and is quite time-consuming.

A method for directly visualizing and counting individual viruses is *transmission electron microscopy*, TEM. An electron beam focused with magnetic field is used for probing and imaging the sample. Virus concentrations can then be determined with image analysis or visual inspection. The need of ultrathin samples, extensive coating and sample preparation in combination with high equipment cost are some draw-

backs of this method. However, there is no need of specific reagents for recognizing the pathogen [26].

Another strategy is to measure and detect viral genetic material. In the 1970s, the polymerase chain reaction, PCR, was developed which enabled multiplication of single DNA strands. PCR has had a great impact on viral detection. The methods have in common that PCR is used for amplifying DNA or RNA to sufficiently high concentrations. Then fluorescent probes that bind to amplified DNA or RNA can be added for detection. Since the amount of DNA or RNA is amplified, very low concentrations can be detected [27]. Weltzel et al. have reportedly detected 560 copies/ml (1 aM) for hepatitis virus with real-time PCR [28]. Drawbacks of PCR based methods are the need of operator skills, sample preparation and long processing time [29].

Many modern surface based detection methods uses some kind of "sandwich" setup, where an antibody or reagent is immobilized on a surface [30]. The target virus then attaches and this is detected in one way or another. A popular biosensor using this setup is the enzyme-linked immunosorbent assay, ELISA [31]. First developed in the 1970s, ELISA exist in many variants, but for the sandwich variant the fundamental idea is having an antibody first immobilized on a surface. Adding a solution containing an antigen (virus) results in the antigens being linked to the antibodies. Additional antibodies results in the forming of antibody-virus-antibody complexes. Addition of a secondary, fluorescently labelled antibody that attaches to the primary antibody create a "sandwich" structure, which enables measuring the amount of antigens via the intensity from the fluorescent marked attached antibodies. The fluorescent signal is often enhanced by adding an enzyme to the solution. Figure 3.1 shows an illustration of an ELISA sandwich setup.

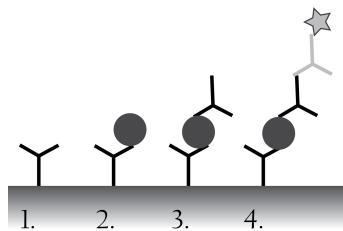


**Figure 3.1:** *Illustration of virus detection with a sandwich ELISA. An antibody is immobilized on a surface (1 in the illustration) before adding viruses which attaches to the antigen (2). Additional antibodies are added, forming antibody-virus-antibody complexes (3). Finally secondary antibodies are added (4), which can be detected by measuring for example the amount of fluorescence.*

## 3.2 Idea of colocalization assay with dual-colour fluorescence microscopy

The detection method investigated in this thesis, named the colocalization assay, is based on the interaction in a solution between SV40 VLPs and fluorescently labelled vesicles also containing GM1. This section aims to give an introduction to the fundamental ideas of the assay.

In a solution containing vesicles and VLPs, the particles will diffuse freely and spontaneously encounter each other. A SV40 VLP sufficiently close to a vesicle with GM1 will specifically bind to the vesicle and they will start to diffuse together. As the whole surface of SV40 is covered by the protein that interacts with GM1, it is plausible that one SV40 can attach to several vesicles. This idea is further expanded by having half of the vesicles labelled with one fluorophore, and the other half labelled with another dye. The fluorophores are chosen to have clearly separated excitation spectra so that they are excited by lasers of different wavelengths. If both a red and a blue vesicle attaches to a VLP, the red and the blue vesicle will start to move together. The idea is illustrated in Figure 3.2. In a microscope with the possibility to separate light emitted by red vesicles and by blue vesicles, the particles can be tracked separately and events where a blue and a red vesicle move in a correlated way can be identified.

Two vesicles can attach to a VLP in three ways: two red vesicles, two blue vesicles or one red and one blue. By combinatorics, the probability of forming a complex of one red and one blue vesicle will be as likely as forming a complex with two red *or* two blue vesicles. It is also likely that larger complexes can form, by having a VLP attaching to more than two vesicles, or by having several VLPs attaching to one vesicle. Configurations including at least one red and one blue vesicle should be detected in the colocalization analysis.

### 3.2.1 Past studies with dual-colour microscopy colocalization

Some earlier studies have been performed with different colour-coded particles and imaging with fluorescence microscopy. For example, Agrawal et al. [32] used colour-coded nanoparticles to detect biomolecules such as nucleic acids. The nanoparticles were functionalized so that red and green nanoparticles could recognize two binding sites on a biomolecule. By applying a solution of nanoparticles and DNA targets to a coverslip and letting it dry, the particles could be imaged with fluorescence microscopy to detect colocalization events with high resolution. Ho et al. have used a similar approach to detect DNA targets [33]. Using three kinds of colour-coded functionalized quantum dots, they have detected three different DNA targets simultaneously.

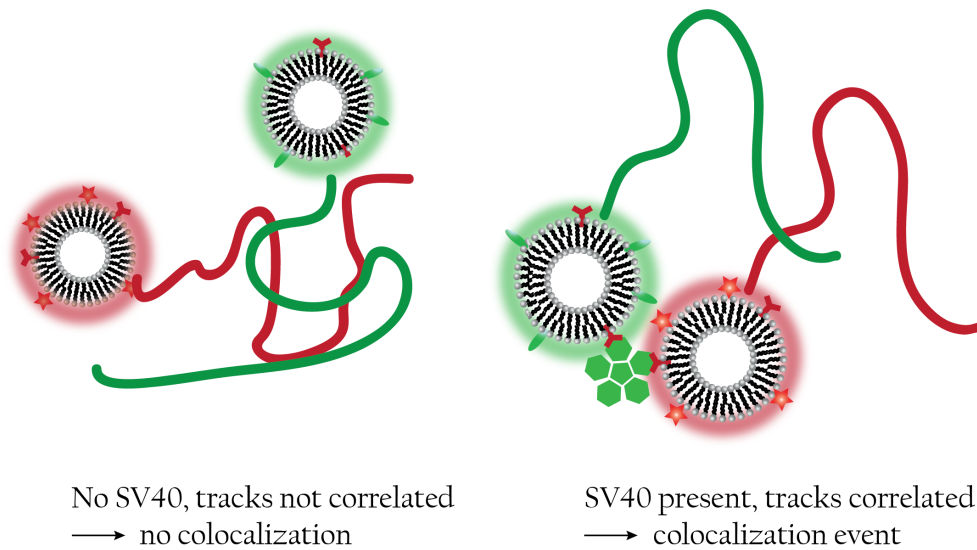


**Figure 3.2:** *The basic idea of the colocalization assay. Fluorescently labelled vesicles diffuse freely in solution together with virus like particles (VLPs). When a VLP (illustrated by the green pentagons) encounters a vesicle, the VLP and vesicle will interact and start to move together. With several vesicles attached to the same VLP, the movement of the vesicles will be correlated. Having two populations of fluorescently labelled vesicles, with well separated excitation and emission spectra, enables tracking of the vesicles separately and detecting complexes with both a red and a blue (green in the figure) vesicle.*

# 4

## Theoretical aspects

IT IS OFTEN VALUABLE to do a theoretical estimation of parameters that are to be experimentally decided. Sometimes rough simplifications are needed in order to do estimates, but one can nevertheless gain valuable insights about the system which could be used when designing further experiments. In this chapter some theoretical aspects considering the collision frequency in solution and the lowest virus concentration that could be detected will be discussed.

### 4.1 Collision frequency in solution

One of the fundamental ideas with the colocalization assay is that vesicles and virus particles collide and form complexes. An estimation of the collision frequency between particles in a solution as a function of concentration can give an idea of the timescale of complex formation, and thus an idea of whether it is fair to expect that colocalization events should be detected in reasonable time.

Small particles suspended in a solution will move according to Brownian motion, driven by continuous collisions with the solvent molecules. In each time step a particle will displace a random distance in a random direction. This type of movement is called *diffusion* and the speed of which this occurs is governed by the Stokes-Einstein equation:

$$D = \frac{kT}{6\pi\eta R}, \quad (4.1)$$

where  $D$  is the diffusion coefficient,  $k$  Boltzmann's constant,  $T$  the temperature,  $\eta$  the viscosity of the medium and  $R$  the radius of the particle [8]. For example, a vesicle represented by a sphere with the radius 50 nm diffusing freely in water, will have a diffusion coefficient of approximately  $4.3 \mu\text{m}^2 \text{s}^{-1}$ . The diffusion coefficient is related to the mean squared displacement,  $\langle r^2 \rangle$ , as

$$\langle r^2 \rangle = 2NDt, \quad (4.2)$$

in  $N$  dimensions, where  $t$  is the time. The mean squared displacement hence grows linearly with time.

For estimating the time scale of collisions between VLPs and vesicles the diffusion equation is solved in three dimensions for two sets of particles: vesicles with radius  $R_{ves}$ , diffusing around a target VLP, with radius  $R_{VLP}$ . The diffusion equation reads

$$\frac{\partial c_{ves}}{\partial t} = D_{VLP,ves} \nabla^2 c_{ves}, \quad (4.3)$$

where  $c_{ves}$  is the concentration of vesicles and  $D_{ves,VLP}$  is the diffusion coefficient of vesicles relative the target VLP, equal to the sum of the independent diffusion rates for vesicles and VLPs. At the steady state, where  $\partial c_{ves}/\partial t$  equals 0, equation 4.3 can be written as

$$D_{ves,VLP} \nabla^2 c_{ves} = D_{VLP,ves} \frac{1}{r^2} \frac{\partial}{\partial r} \left( r^2 \frac{\partial c_{ves}}{\partial r} \right) = 0, \quad (4.4)$$

in spherical coordinates. The solution to this equation is

$$c_{ves}(r) = \frac{A}{r} + B, \quad (4.5)$$

where  $A$  and  $B$  are constants. This equation describes the concentration of vesicles at the distance  $r$  from the centre of the VLP. Two boundary conditions can now be used: The first as the bulk concentration of vesicles as the boundary condition for  $r_\infty$ , and secondly assuming that the concentration of vesicles is zero at the distance where vesicles and VLPs touch, i.e. at  $r = R_{VLP} + R_{ves} = R_{ves,VLP}$ . The constants in equation 4.6 can then be replaced:

$$c_{ves}(r) = \left( 1 - \frac{R_{VLP,ves}}{r} \right) c_{ves,\infty}, \quad (4.6)$$

where  $c_{ves,\infty}$  is the bulk concentration of vesicles. The collision rate is the flux,  $\vec{j}$ , of vesicles towards VLPs at the distance  $R_{ves,VLP}$ , multiplied by the surface area of a sphere with radius  $R_{ves,VLP}$ . The flux is calculated from Fick's law which reads:

$$\vec{j} = -D_{ves,VLP} \vec{\nabla} c_{ves}. \quad (4.7)$$

Inserting  $c_{ves}$  from equation 4.6, we get

$$\vec{j} = -D_{ves,VLP} \frac{R_{ves,VLP}}{r^2} c_{ves,\infty}. \quad (4.8)$$

The total flux is thus

$$J(j \rightarrow i) = 4\pi R_{ves,VLP}^2 \cdot D_{ves,VLP} \frac{R_{ves,VLP}}{R_{ves,VLP}^2} c_{ves,\infty} = 4\pi D_{ves,VLP} R_{ves,VLP} c_{ves,\infty}. \quad (4.9)$$

Inserting the expression for diffusion coefficients in equation 4.1 yields

$$J(j \rightarrow i) = \frac{2 kT}{3 \eta} \left( 2 + \frac{R_{VLP}}{R_{ves}} + \frac{R_{ves}}{R_{VLP}} \right) c_{ves, \infty}, \quad (4.10)$$

which can be interpreted as the number of  $j$ -particles colliding with a  $i$ -particle per time unit. Inserting numerical values of the radii of the vesicles and VLPs as  $R_{ves} = 50$  nm,  $R_{VLP} = 20$  nm,  $\eta = 0.001$  Pa s as the viscosity of water, the temperature  $T = 300$  K and a bulk concentration of vesicles of 10 pM gives a collision rate  $J(j \rightarrow i)$  of approximately  $0.015$  s<sup>-1</sup>. The characteristic time scale of collisions is the inverse of this value, i.e. 70 seconds. With a bulk concentration of vesicles of 1 pM, the characteristic time becomes ten times longer, i.e. 700 s. With the VLPs having a very strong affinity towards GM1 in the vesicles, most collisions would be expected to result in an interaction and binding.

## 4.2 Diffusion of aggregates

As was discussed in the previous section, a VLP diffusing freely in a solution containing vesicles will every now and then encounter vesicles, resulting in attachment and formation of a complex. An interesting question to pose is how this affects the diffusion rate and the measured radius. By approximating a simple complex consisting of two attached particles with an ellipsoid with the axis diameters  $(a, b, b)$ , the diffusion rate for this complex can be estimated. Ellipsoids have different diffusion coefficients along different axis, whereas for a sphere the diffusion is isotropic [34]. An approximation for the diffusion coefficients for an ellipsoid is given by

$$D_a = \frac{k_B T [\ln(2c) - 0.5]}{2\pi\eta a}, \quad (4.11)$$

$$D_b = \frac{k_B T [\ln(2c) + 0.5]}{4\pi\eta a}, \quad (4.12)$$

where  $D_a$  and  $D_b$  are the diffusion coefficients corresponding to the semiaxes  $a$  and  $b$  and  $c$  is the ratio  $a/b$  [35]. Inserting some numerical values for  $a = 200$  nm and  $b = 100$  nm, as an approximation for two attached particles, each with a diameter 100 nm, yields  $D_a = 2.9$  μm<sup>2</sup>/s and  $D_b = 3.1$  μm<sup>2</sup>/s. This can be compared with the earlier calculated diffusion coefficient for a sphere with a diameter of 100 nm,  $4.3$  μm<sup>2</sup>/s. The two diffusion coefficients for this ellipsoid are thus approximately 30 % smaller than the diffusion coefficient for a sphere with the same diameter as the short axis of the approximated ellipsoid.

Another effect is that ellipsoids can have different orientations in three dimensions, whereas a microscope records the ellipsoids in two dimensions. This means the diffusion in the microscope's  $x$  and  $y$  direction will depend on the orientation of the ellipsoid.

To conclude, aggregation in a solution should induce an increase of the measured radius which should be reflected in the distribution of the radius.

### 4.3 Theoretical limit of detection

For estimating a theoretical limit of detection, we assume that all SV40 VLPs attaches to strictly two vesicles. Hence, with twice as many vesicles as VLPs, all vesicles should ideally form complexes with VLPs. The formation of larger complexes will most likely occur, but for estimating the maximum colocalization frequency we make this assumption. In order to be detected by the colocalization analysis, a complex need to comprise at least one red vesicle and at least one blue vesicle.

We define a "colocalization frequency" as:

$$F = \frac{\text{number of colocalization events}}{\text{number of free vesicles} + \text{number of colocalization events}} \quad (4.13)$$

where  $0 < F < 1$ . Denoting the concentration of VLPs as  $[VLP]$  and the total vesicle concentration as  $[V]$  this can be written more compactly. The number of colocalization events is ideally  $[VLP]$  and with each VLP attaching to two vesicles, the number of free vesicles is  $[V] - 2 \cdot [VLP]$ . However, roughly half of the complexes would consist of two vesicles of the same colour, and is thus invisible in the colocalization analysis, so we multiply with 0.5. This yields

$$F = \frac{0.5 \cdot [VLP]}{[V] - 2 \cdot [VLP] + [VLP]} = \frac{0.5 \cdot [VLP]}{[V] - [VLP]}. \quad (4.14)$$

This would thus be the highest theoretical value of the colocalization frequency for a sample. For example with  $[V] = 10$  pM and  $[VLP] = 0.1$  pM, the colocalization frequency would be 0.5 %. Hence, the limit of detection is determined by the noise level and is also affected by for example unspecific interactions, i.e. the colocalization frequency for control experiments with  $[VLP] = 0$ .

The maximum concentration of VLPs that could be resolved according to this model would then be half of the vesicle concentration, i.e. 5 pM. However, these statements hold if the VLPs and vesicles only form complexes with one VLP and two vesicles. Forming larger complexes with several VLPs and vesicles is not only possible, but plausible. A concentration of 5 pM will thus not be enough to yield the maximum number of colocalization events. The former statement about the limit of detection is most probably an underestimation, presumably considerably higher concentrations of VLPs are needed for detection.

# 5

## Materials and methods

NUMEROUS INSTRUMENTS and techniques exist for characterizing biological entities, determining physical parameters and imaging particles and molecules. This chapter gives a brief explanation of the different methods and instruments used in the project. The first section covers the fabrication of the vesicles used in all experiments. The vesicles are also characterized in terms of emission and absorption spectra. The second section introduces the QCM-D technique which was used to verify that the desired interactions occur between the vesicles and SV40. The following section describes Nanoparticle Tracking Analysis which was used to characterize the size of the vesicles and as a reference technique for investigating the interaction between vesicles and SV40. The last sections covers the colocalization assay, explaining the experimental setup and the data analysis.

### 5.1 Preparation of vesicles

The vesicles used in all experiments consisted of 98 wt% POPC lipids, 1 wt% DOPE lipids with fluorescent molecules and 1 wt% percent lipids with GM1 receptors. Two different fluorescent markers were used; ATTO488 and ATTO633. These hydrophilic fluorophores have a high fluorescence quantum yield, high thermal and photo-stability [36, 37]. The two kinds of vesicles are hereafter called "blue vesicles" and "red vesicles", due to their absorption of blue and red light, respectively. However, the blue vesicles emit green light, therefore they are green in the figures.

For preparing vesicles, the lipids, GM1 and the fluorescent markers were mixed and dried with nitrogen and in a vacuum pump. This removed the chloroform that the lipids were dissolved in for storage. The dry mixture of POPC lipids, GM1 and DOPE lipids was then dissolved in a buffer called PBS and vortexed, which induce self assembly into vesicles. For ensuring homogenous, unilamellar vesicles the solution containing vesicles was pushed through a membrane with 30 nm pores in a so-called *extruder*. Since vesicles are flexible and can deform without breaking, they can deform and squeeze through pores much smaller than themselves. Therefore, the remaining vesicles are larger than 30 nm, rather approximately 100 nm in diameter.

### 5.1.1 Determination of excitation and emission spectrum for fluorophores

For determining excitation and emission spectrum of a fluorophore, a *spectrofluorometer* is a convenient instrument to use. A spectrofluorometer measures emission and excitation of a sample at different wavelengths [38]. The sample is exposed to light to excite the fluorophores. Two monochromators enables exciting with photons of one wavelength and collecting photons at another wavelength. For determination of the emission spectrum, a fixed wavelength is chosen for excitation of the sample. A scan is then performed over a range of emitted wavelengths, measuring the emission at each wavelength, producing a spectrum. For determining the excitation spectrum, the measurement is performed the other way around, a fixed emission wavelength is chosen and the absorbance is measured over a range of excitation wavelengths.

## 5.2 Quartz-crystal microbalance with dissipation monitoring

Quartz-crystal microbalance with dissipation monitoring, QCM-D, is a label-free, high-sensitivity surface monitoring technique. It is an acoustic biosensing technique which can be used for measuring adsorbed mass on a surface with a sensitivity of up to 1 ng/cm<sup>2</sup>, but also for modelling structural properties like elasticity and viscosity of the adsorbed material [10, 39, 40]. In this project QCM-D was used to confirm that SV40 binds specifically to vesicles.

The fundamental basis of QCM-D is the piezoelectric property of quartz [41]. A phenomenon called *the piezoelectric effect* (from *piezo-* to squeeze or press) causes the crystal to expand when applying an external electric field. An alternating applied field will cause the piezocrystal to oscillate, with resonance for certain frequencies of the applied field. These frequencies consists of a fundamental frequency and its odd harmonics. By cutting the quartz crystal along certain specific planes, the oscillation will be in shear mode [41], which is illustrated schematically in Figure 5.1. When a mass is added to the surface, the resonance frequency will change and this shift in frequency can be monitored over time. Information about events at the surface, such as the added mass, can be calculated with the Sauerbrey equation:

$$\Delta m = -\frac{C\Delta f}{n}, \quad (5.1)$$

where  $\Delta m$  is the change in adsorbed mass (per area unit),  $\Delta f$  is the change in resonance frequency and  $n$  is the number of the harmonic used.  $C$  is a material constant, which for the 5 MHz crystal used is 17.7 ng cm<sup>-2</sup> Hz<sup>-1</sup> [42]. However, one

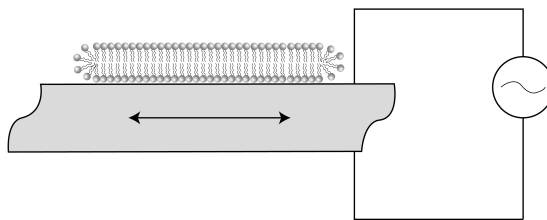


**Figure 5.1:** Schematic illustration of the oscillation of the quartz crystal. When applying an alternating voltage the crystal oscillates in a shear mode as the arrow indicates.

limitation is that this equation only holds for rigid, evenly distributed and sufficiently thin layers of adsorbed molecules.

The part of the name "with dissipation monitoring", refers to another part of the measurement: a measure of energy losses. A more rigid material, such as a lipid bilayer, do not lose much energy between oscillations and have thus a low dissipation. A more viscous material, for example a lipid bilayer with large molecules attached, have a larger energy loss and a higher dissipation. Monitoring the dissipation can thus give information about the characteristics of the material attached to the surface [41].

The QCM-D device provides the frequency shift and dissipation for the six first odd harmonics. These harmonics have different sensitivity profiles i.e. different distances affects the resulting shift. Higher harmonics are more sensitive near the surface [40].

### 5.3 Nanoparticle tracking analysis

Nanoparticle tracking analysis, NTA, is a technique to characterize particles suspended in solution by tracking the Brownian motion of each particle. The NTA setup is shown schematically in Figure 5.2. The particles are suspended in liquid in a sample chamber and undergo Brownian motion, i.e. a random movement due to collisions between the particles and water molecules [43]. As a laser beam is passed through the sample chamber the particles scatter light as they diffuse through the liquid. A camera captures the scattered light and the movement of the particles can be tracked individually with a software. The two-dimensional projection of the movement in three dimensions is calculated and the diffusion coefficient  $D$  can be calculated according to:

$$D = \frac{z_{2D}^2}{4t}, \quad (5.2)$$

where  $z_{2D}^2$  is the mean-square displacement in two dimensions and  $t$  is the time. With an estimation of  $D$ , the hydrodynamic radius can be calculated with Stokes-

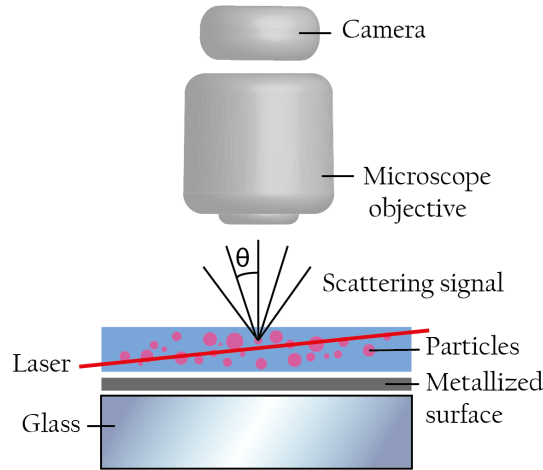


**Figure 5.2:** Schematic illustration of the setup of a NTA device. The sample is put in a chamber on top of a partly metal coated prism. A laser beam is passed through the sample and the scattered signal is collected by a CCD camera.

Einstein's formula;

$$D = \frac{k_B T}{6\pi\eta R}, \quad (5.3)$$

where  $k_B$  is Boltzmann's constant,  $T$  is the temperature,  $\eta$  the viscosity of the medium and  $R$  the radius of the particle [8]. The radius  $R$  is calculated for all particles that is tracked during sufficiently long time, resulting in a size distribution.

Commercial instruments for NTA have slightly different designs. *Malvern Technologies*, which produces the instrument used in this project, uses a prism partly coated with metal to achieve a low angle of illumination. Modern NTA devices also have the ability to track fluorescent particles, by adding a filter that only transmits light of certain wavelengths corresponding to the emission of the used fluorophore. This can for example be used for distinguishing specific particles in a mixture [44]. The size range for particles that can be characterized in terms of size is 30 to 1000 nm [43, 45].

For achieving good statistical results, the choice of concentration of particles is important in NTA. A high concentration provides more data, but also causes overlapping of particle tracks and higher background noise. Particle overlapping leads to losing track of the particle which lowers the accuracy. A suitable choice of concentration is  $10^7$  to  $10^9$  particles/ml, corresponding to  $10^{-14}$  –  $10^{-12}$  M [45].

In this project, NTA was used to measure the size of the vesicles, to do some initial experiments with VLPs and vesicles and to see if the complexes formed by VLPs and vesicles have a significant effect on the size distribution.

## 5.4 Colocalization assay

The colocalization setup has been the main focus of this thesis, and it is in some ways similar to that of the commercial NTA device. It basically consists of a microscope with a objective with a magnification of 63 and a sample holder with particles suspended in liquid. An illustration of the experimental setup is shown in Figure 5.3. The particles are imaged and recorded by a camera, and the data is analysed with a software to extract individual particle tracks. From these, the degree of colocalization can be determined by identifying correlated tracks.

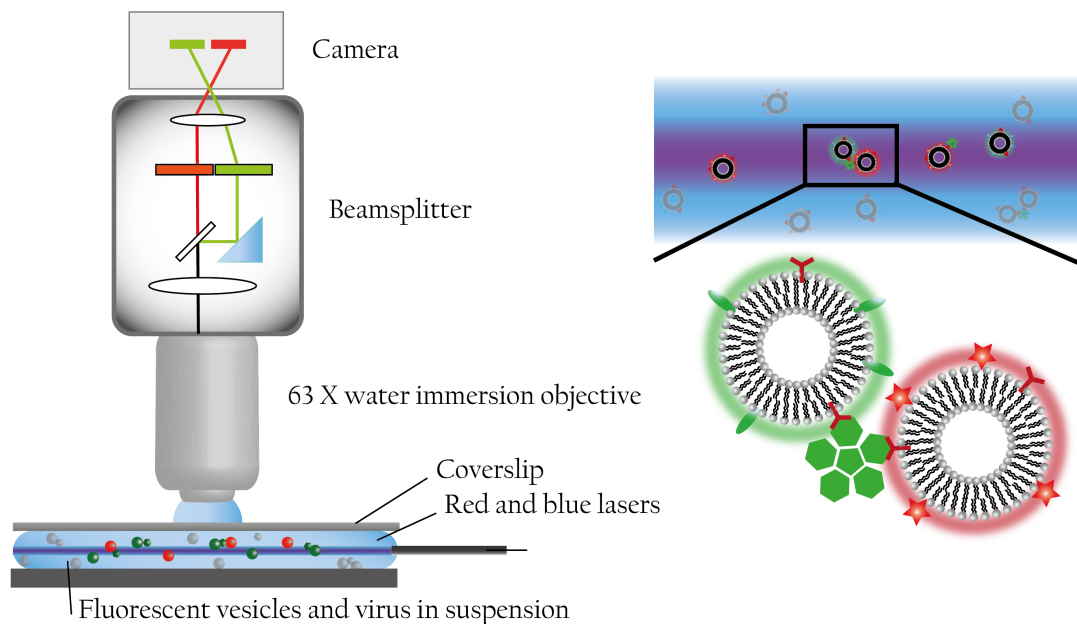


**Figure 5.3:** Schematic illustration of the experimental setup for colocalization assay. The sample containing blue and red vesicles and virus is injected into a channel in a PDMS mould. A fibre is mounted in the channel, simultaneously illuminating parts the sample with blue and red laser with wavelengths 488 nm and 635 nm, respectively. A dichroic mirror in the beamsplitter separates the emitted light into long and short wavelengths, and two filters only transmits light with certain wavelengths into the camera. In that way the emitted light is separated into two channels. A CCD camera records the illuminated vesicles in the two channels separated. The two channels can be overlaid in a software, finding colocalization events (right).

A PDMS mould with a thin channel is used for containing the sample, illustrated from above in Figure 5.4. A laser fibre is mounted into the channel, illuminating the sample and enabling visualization of particles. The fibre had a 50  $\mu\text{m}$  core which enabled a broad illumination of the channel. Any colour of laser can be used, and several colours can be used simultaneously. This is a difference from the NTA device, where only one laser at a time can be used. The sample volume is approximately 100  $\mu\text{l}$  of which approximately 1/1000 is illuminated by the laser beam. In the experiments in this thesis, a blue laser with wavelength 488 nm was

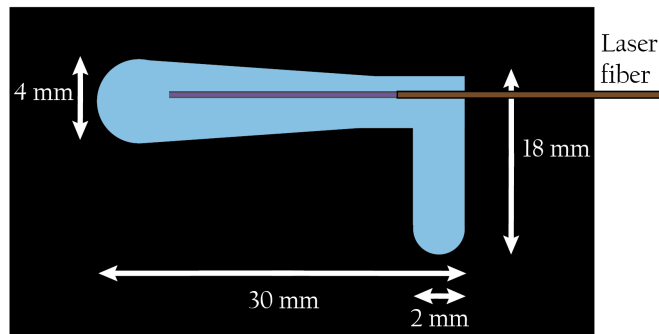


**Figure 5.4:** Top view of the sample holder. It is made of a black silicon-based polymer (PDMS) with a thin channel (light blue in figure) where the sample is placed. The fibre was mounted in the channel as illustrated, illuminating part of the sample. On top of the sample holder a glass slide is placed to seal the channel.

used for exciting the blue fluorophores (ATTO488), and a red laser with wavelength 635 nm for exciting the red fluorophores (ATTO633). The lasers could be controlled separately, enabling changing the intensities of the lasers independently.

The microscope was used in fluorescence mode, with a beamsplitter and two filters separating the light into two channels, hereafter called "blue channel" and "red channel". The pathway of the light in the microscope is shown schematically in the upper part of Figure 5.3. As the fluorophores are excited by the two lasers they emit light with different wavelengths, as well as scattered light. The beam splitter transmits light with wavelength longer than 560 nm and reflects light with shorter wavelength. The light with shorter wavelength is reflected once more at a mirror. Two filters then allows light with certain wavelengths to pass ( $535 \pm 25$  nm and  $700 \pm 38$  nm for the blue and red channel, respectively). The filters were chosen to match the emission spectra for the fluorophores.

The data was collected with a CCD camera in form of movies consisting of 1000 consecutive frames (exposure time: 33 ms, time between frames: 1 ms) which could then be analysed in for example Matlab. The two channels are illustrated in Figure 5.5, which is an example of a frame from an experiment with red and blue vesicles excited by both lasers simultaneously. Vesicles are seen as bright dots, whereas vesicles out of focus appear as diffuse rings.

### 5.4.1 Choice of objective

When performing single-particle tracking, it is desired to track the particles for as many frames as possible as this makes it easier to distinguish between true and false colocalization events. The number of frames that a particle can be tracked depends on the time a particle is in focus which is strongly dependent on the depth of field. The depth of field can be described as

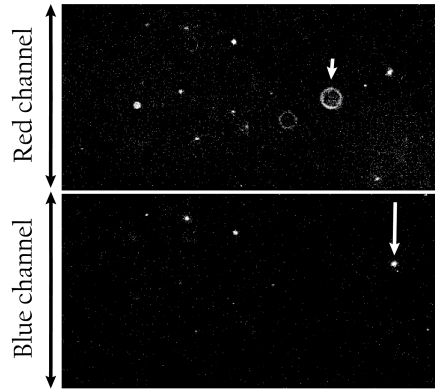


**Figure 5.5:** Snapshot from a movie from an experiment with both blue and red vesicles in the sample, excited by both red and blue lasers. The upper half of the figure corresponds to red vesicles, and the lower half corresponds blue vesicles. Vesicles in focus appear like bright dots, as indicated by the long arrow. Vesicles out of focus appear like larger circles, as indicated by the short arrow.

$$d_{tot} = \frac{\lambda_0}{n_0(\text{NA}/n_0)^2} + \frac{e}{(\text{NA}/n_0)M}, \quad (5.4)$$

where  $\lambda_0$  is the exciting wavelength,  $n_0$  is the refractive index surrounding the objective, NA is the numerical aperture,  $e$  is the smallest distance that can be resolved by a detector placed in the image plane of the microscope and  $M$  is the total magnification of the objective. In Figure 5.6, the depth of field is plotted for three types of objectives, with different magnifications and surrounding media. The water immersion objective used in the experiments had a magnification of 63 and a numerical aperture of 0.9, which corresponds to a depth of field of  $0.9 \mu\text{m}$ .

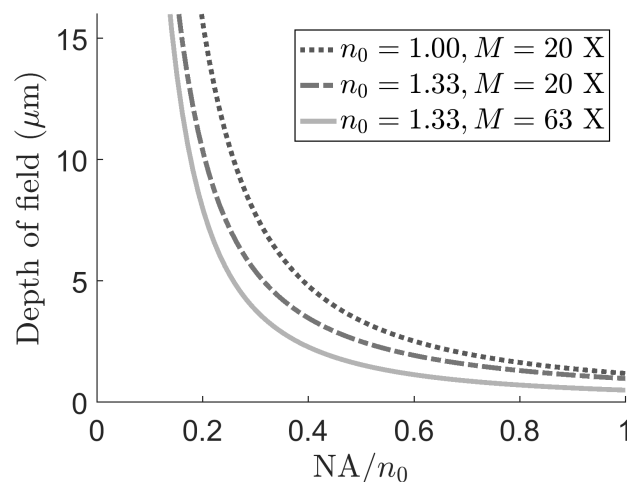


**Figure 5.6:** Depth of field for three different objectives, with different magnifications and surrounding media. For  $n_0 = 1.33$ , the surrounding medium is water, for  $n_0 = 1.00$ , the surrounding medium is air. The objective used in experiments had  $n_0 = 1.33$ ,  $M = 63$  and  $\text{NA}/n_0 = 0.67$ , thus a depth of field of  $0.9 \mu\text{m}$  with  $e = 14 \mu\text{m}$ .

## 5.5 Data analysis

To count the number of colocalization events in the data a set of Matlab scripts written by Stephan Block were used. In the analysis, vesicles are identified and tracked throughout the movies recorded in the colocalization experiments. The colocalization events are identified by finding vesicles with a correlated movement. A flowchart illustrating the main parts in the algorithm is shown in Figure 5.7.

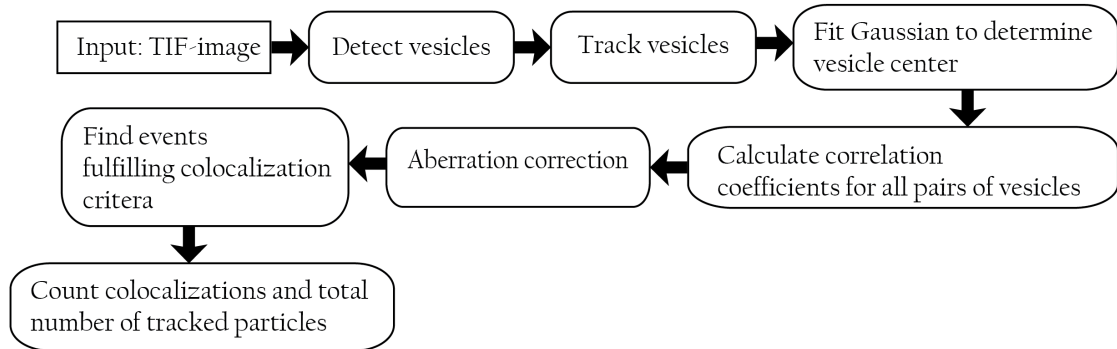


**Figure 5.7:** A flowchart emphasizing the main steps in the data analysis.

In the first step, vesicles are detected in each frame by finding local intensity maxima. By applying a global threshold, the local maxima representing the vesicles are found. Vesicles are then tracked by matching particles in a frame  $N$  with particles in frame  $N - 1$ . This is done by calculating the distances between particles in frame  $N - 1$  and  $N$  and match the closest ones. Since vesicles are diffusing in and out of focus, and in and out of the field of view, most vesicles are not visible during the whole movie. Each tracked vesicle is identified with a  $x$ -coordinate and a  $y$ -coordinate for each frame that the specific vesicle is visible in. By fitting a two-dimensional Gaussian distribution to the intensity of each particle the centre of mass of each particle is calculated with subpixel resolution in each frame.

In the last step the colocalization events are identified. The criteria for a colocalization event can be summarized as one particle in the red channel and one particle in the blue channel fulfilling the following criteria; 1) the particles should be at the same position at the same time, 2) the tracks should be long enough and 3) the tracks should be similar enough.

The third, criteria is determined by calculating a measure of the correlation for each red and each blue particle appearing in the same time frames. The correlation calculations are derived from Cauchy-Schwartz inequality which states

$$\left| \sum_{i=1}^n a_i b_i \right|^2 \leq \sum_{i=1}^n |a_i|^2 \sum_{i=1}^n |b_i|^2 \quad (5.5)$$

Dividing with the right hand side gives

$$\frac{\left| \sum_{i=1}^n a_i b_i \right|^2}{\sum_{i=1}^n |a_i|^2 \sum_{i=1}^n |b_i|^2} \leq 1 \quad (5.6)$$

This is equal to 1 if and only if  $a_i = b_i$ . We introduce two parameters  $\rho_x$  and  $\rho_y$  defined by:

$$\rho_x = \frac{\left| \sum_{i=1}^n \Delta r x_i \Delta b x_i \right|^2}{\sum_{i=1}^n |\Delta r x_j|^2 \sum_{i=1}^n |\Delta b x_j|^2} \quad (5.7)$$

$$\rho_y = \frac{\left| \sum_{i=1}^n \Delta r y_i \Delta b y_i \right|^2}{\sum_{i=1}^n |\Delta r y_j|^2 \sum_{i=1}^n |\Delta b y_j|^2}, \quad (5.8)$$

where  $\Delta r x$  and  $\Delta r y$  is the displacements in the x- and y-direction, respectively, for a particle in the red channel between two particles in two consecutive frames. In the same way,  $\Delta b x$  and  $\Delta b y$  are the displacements for a particle in the blue channel in the same time frames.  $n$  is the number of frames that the particle is visible in.  $\rho_x$  and  $\rho_y$  are calculated for all potentially colocalized particles, i.e. all particles that appear in the same time frames. An example of the correlation coefficient is shown in Figure 5.8 where two simple examples are shown. In subfigure A,  $\rho_x$  and  $\rho_y$  are calculated for two similar tracks, whereas in subfigure B,  $\rho_x$  and  $\rho_y$  are calculated for two more different tracks. For simplicity, the example tracks are much shorter than tracks obtained in the experiments.

The larger the deviation is between the tracks of the red and the blue particle, the lower the values of  $\rho_x$  and  $\rho_y$  and the lower the probability that they are truly correlated. Hence, the next step in the data analysis is to compare  $\rho_x$  and  $\rho_y$  to a threshold,  $\rho_{\min}$ . If both are larger than the threshold, the particular red and blue particle are initially classified as colocalized.

Then a position criteria is applied to the particles. If the mean distance between a red and a blue particle is larger than  $d_{\max}$  pixels, it is unlikely that they are attached to each other and this event is rejected. An aberration correction is also applied to account for imperfections in the imaging system. The correction will be described more detailed in the next section.

The colocalization frequency for each measurement is then calculated with equation 4.13.

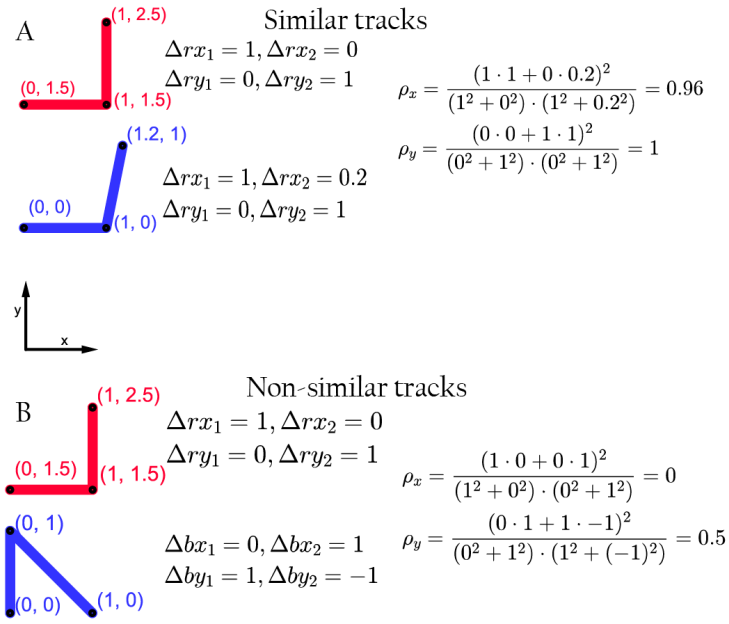


**Figure 5.8:** Illustration of how the correlation coefficients,  $\rho_x$  and  $\rho_y$ , are calculated. The red and the blue lines corresponds to a three-frame track from a red and a blue vesicle, respectively. In subfigure A, the correlation coefficients  $\rho_x$  and  $\rho_y$  are calculated for two similar tracks, whereas in subfigure B,  $\rho_x$  and  $\rho_y$  are calculated for two more different tracks. As can be seen,  $\rho_x$  and  $\rho_y$  for subfigure A is larger than  $\rho_x$  and  $\rho_y$  for subfigure B.

### 5.5.1 Aberration correction

In the output images from the microscope, the red and blue channels are positioned in the upper and lower half of the image, respectively. If the imaging system was perfect, a pixel in a red channel should correspond to a pixel in the blue channel according to:

$$b_x = r_x \quad (5.9)$$

$$b_y = r_y + p_{\max}/2, \quad (5.10)$$

where  $r_x$  is the  $x$ -coordinate of a pixel in the red channel and  $b_x$  the corresponding pixel in the blue channel,  $p_{\max}$  the height of the image in pixels and  $r_y$  and  $b_y$  the  $y$ -coordinates of the two channels. However, due to imperfections in the imaging system, there are some small aberrations in the imaging and equation 5.9 and 5.10 do not hold exactly for all pixels. To account for these anomalies an aberration correction is determined by first choosing the colocalization events that are most likely to be truly correlated, i.e. have high values of  $\rho_x$  and  $\rho_y$ . These events are used to determine the deviation in pixels between the red and the blue channels. For example, if the positions in  $x$ - and  $y$ -directions are  $(10,10)$  in one channel and  $(10,270)$  in the other channel in a colocalization event, with  $p_{\max} = 512$ , the

deviation at that position is 0 in the  $x$  direction and 4 in the  $y$  direction. Using many such events, one polynomial for each dimension can be fitted to the data points yielding an aberration correction for  $b_x = f_x(r_x)$  and  $b_y = f_y(r_y)$ .



# 6

## Results

THE EXPERIMENTAL RESULTS will be summarized in this chapter, starting with the confirmation of the interaction between vesicles and VLPs. Then follows characterization of vesicles in terms of size and emission and absorption spectra. In the last sections the experiments with the colocalization assay are presented.

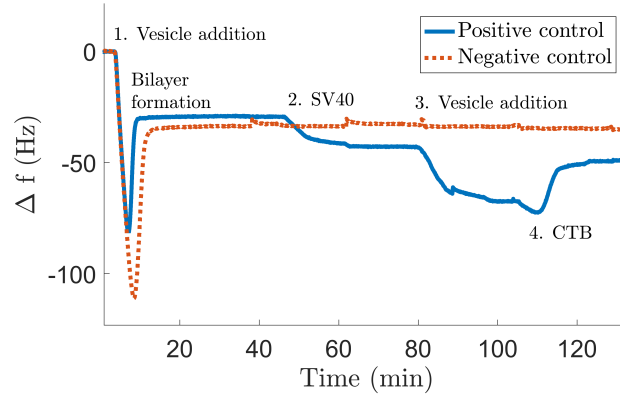
### 6.1 Verification of vesicles-virus interaction

One presumption for the colocalization assay is that SV40 VLPs interact with vesicles and form complexes. A QCM-D measurement was performed to confirm this assumption. In the experiment a bilayer was first formed from vesicles containing the receptor GM1, then virus particles were added to verify binding to GM1. Additional injection of vesicles with GM1 validated additional binding to SV40. Finally, the inhibitor cholera toxin was added to investigate the specificity of the interactions. The response from these different injections for the third harmonic is shown in Figure 6.1, together with an illustration of the different steps. A measurement from a negative control experiment is also plotted, i.e. a measurement with no SV40 injected, but the other steps being the same.

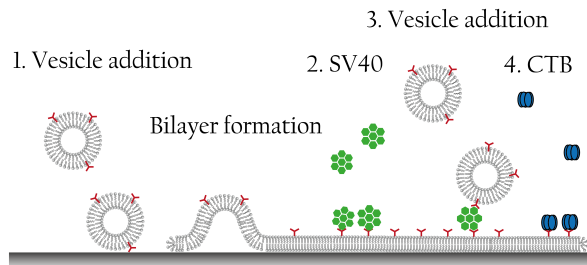
Injecting vesicles initiates an adsorption on the surface (marked 1 in Figure 6.1) resulting in a negative frequency shift. The larger the shift, the more adsorbed vesicles and after a critical coverage, the vesicles rupture and start forming a bilayer. When all vesicles have ruptured a supported lipid bilayer has formed, with a final frequency shift. The difference between the negative and positive control in final values of frequency shift may be a result of using different QCM-D chambers while performing the measurements simultaneously.

When injecting virus particles in the system for the positive control (2 in Figure 6.1), the viruses bind to the GM1 incorporated in the bilayer which increase the negative frequency shift. (Notice that more viruses could have bound to the bilayer if a higher concentration had been used). The signal stabilizes at approximately 60 minutes, and is stable also when rinsed with PBS at  $t \approx 65$  min, indicating that the interaction is very strong. Adding more vesicles (3 in Figure 6.1) leads to larger

negative shifts for frequency for the positive control and to no such response for the negative control. Finally addition of cholera toxin culminates in a rapid increase in frequency shift for the positive control. This supports the assumption that CTB competes with SV40 to bind to GM1 in the bilayer and that SV40 bind specifically to GM1. There is a final frequency shift compared to the control, due to the mass of the CTB. It is also possible that not all vesicles and VLPs are competed out, since the CTB can also attach to the GM1 on the vesicles on top of the VLPs.



(a)



(b)

**Figure 6.1:** (a) A QCMD plot showing the formation of a bilayer and binding of virus particles to the bilayer. The numbers in the figure represents different injections; i.e: 1) Injection of 1 nM vesicles, 2) injection of 70 pM SV40 VLPs, 3) injection of 0.1 nM vesicles, 4) injection of 20 nM CTB. An illustration of the different steps is shown in subfigure b).

## 6.2 Vesicle size distribution and aggregation

A NTA device was used to determine the sizes of the vesicles and also to get an initial idea of how the addition of SV40 to vesicles in solution affects aggregation.

The size distribution is shown in figure 6.2 for blue and red vesicles together with lognormal fits. The blue and red vesicles have significantly different diameters, with mean values of 160 and 120 nm, respectively. The diameters were expected to be

similar for the blue and red vesicles since they were prepared according to the same protocol. The only difference between the vesicles are the fluorophores and it is possible that the diffusion rate, and thus the measured radius is maybe slightly affected by the fluorophore.

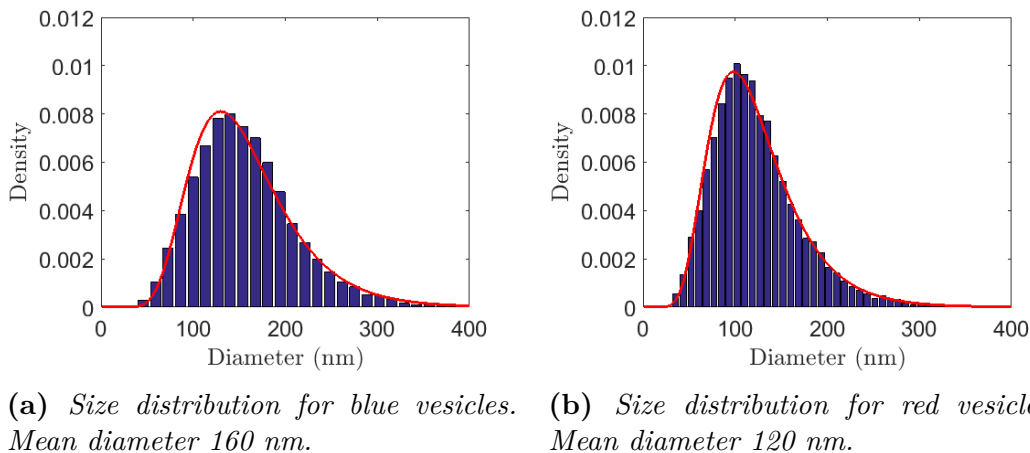


**Figure 6.2:** Size distribution of a) blue vesicles and b) red vesicles. The histograms are shown together with a lognormal fit of the distribution.

To see how the addition of SV40 affects the size distribution, 10 pM red vesicles and 10 pM blue vesicles were incubated for 30 minutes with different concentrations of SV40. Figure 6.3 illustrates the size distribution and mean diameter. In the inserted figure it can be seen that the mean diameter increases with higher SV40 concentration and it seems like already for a virus concentration of 1 pM a statistically significant difference, compared to the control, can be measured.

To deduce whether the means of the control sample and the sample with [VLP]= 1 pM are equal or not the Student's t-test can be used [46]. The test statistic to evaluate whether the population means are equal or not is defined as:

$$t = \frac{\bar{X}_1 - \bar{X}_2}{s_{\bar{X}_1 - \bar{X}_2}}, \quad (6.1)$$

where  $\bar{X}_i$  is the mean for sample  $i$  and

$$s_{\bar{X}_1 - \bar{X}_2} = \sqrt{\frac{s_1^2}{n_1} + \frac{s_2^2}{n_2}}. \quad (6.2)$$

Here  $s_i^2$  is the estimated variance for sample  $i$  and  $n_i$  is the sample size. The statistic  $t$  approximately follows a  $t$  distribution with the number of degrees of freedom calculated as

$$\text{d.f.} = \frac{s_1^4/n_1^2 + s_2^4/n_2^2}{(s_1^2/n_1^2)/(n_1 - 1) + (s_2^2/n_2^2)/(n_2 - 1)}. \quad (6.3)$$

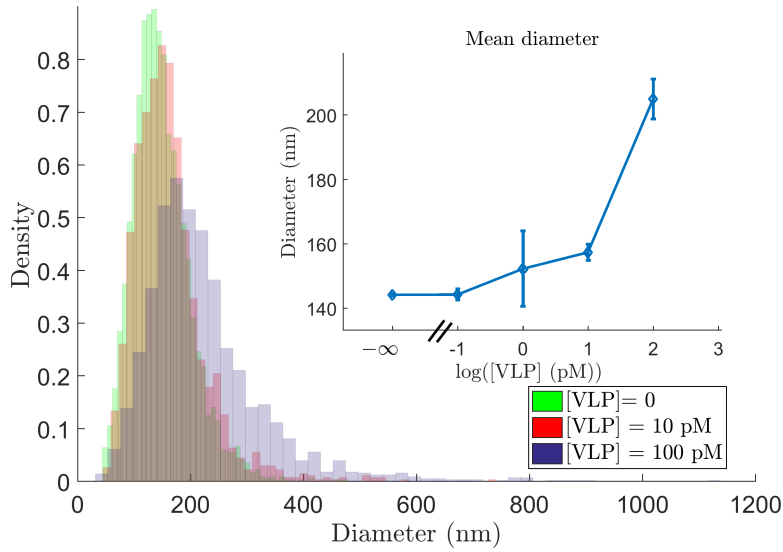


**Figure 6.3:** Size distribution for a mixture of SV40 VLPs and vesicles for different concentrations of VLPs, as well as a negative control with  $[VLP] = 0$ . Inset image: Mean diameter for different VLP concentration, including negative control experiment with  $[VLP]=0$ .

However, this test is applicable to normally distributed samples, and the distributions for the NTA measurements are lognormally distributed. To account for this, the natural logarithm is applied to the samples before calculating the means and variances and inserting values into equation 6.1. Doing so yields a  $t$ -statistic of 3.9 for the negative control and the sample with  $[VLP] = 1$  pM, which compared to the  $t$ -distribution results in the distributions being unequal with a  $p$ -value of less than 0.005, thus with large significance. Doing the same for the control and the sample with  $[VLP]=0.1$  pM yields a  $t$ -statistic of 0.3, which means that these measurements can not be distinguished with significance.

### 6.3 Excitation and emission spectrum for fluorophores

For motivating the choice of filters and beamsplitter in the colocalization setup, discussed in section 5.4, the emission and excitation spectra of the fluorophores were determined with a spectrofluorometer. These spectra are shown in Figure 6.4, together with an illustration of the wavelength intervals corresponding to the two filters. The aim is in the microscope to separate the light emitted from the blue vesicles from the light emitted by red vesicles, and this is facilitated by having distinctly separated emission peaks [47]. As is seen in Figure 6.4, the emission peaks

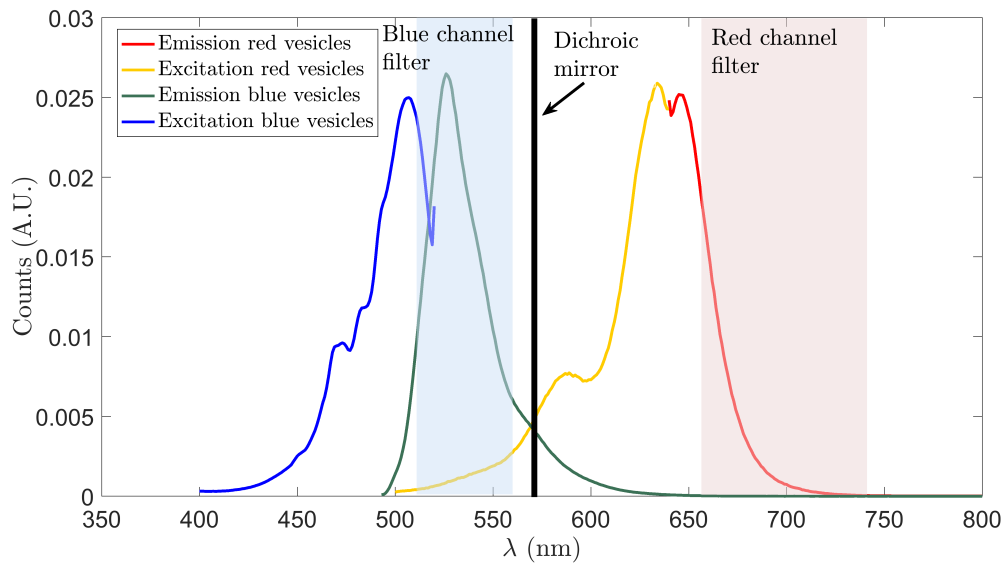


**Figure 6.4:** The normalized absorption and emission spectra for red and blue vesicles, respectively. The coloured rectangles illustrate which wavelengths are transmitted by the filters in the beamsplitter, and the black line indicates the wavelength where the dichroic mirror separates the light.

for the red and the blue vesicles are clearly separated, and the chosen filters seem to correspond well to the emission spectra.

## 6.4 Experiments with colocalization assay

The main part of this project consisted of experiments with the colocalization assay described in section 5.4. The results from these experiments are summarized in the following sections, including some tests of the lasers, determination of the dynamic range of the assay, and an evaluation of the data analysis method.

### 6.4.1 Performance test for colocalization assay

When working with two fluorophores there is a risk of so called *bleed-through*, meaning that one fluorophore is detected in the channel where only the second fluorophore should be visible [47]. In this case, this means that for example a blue vesicle excited by the blue laser could be emitting light in the wavelength range of the red channel. According to the spectra in Figure 6.4, this should be very unlikely. Another potential problem could be so called *cross-talk*, when two fluorophores are excited with the same wavelength of light. In this case, both red and blue vesicles being excited by the red or the blue laser.

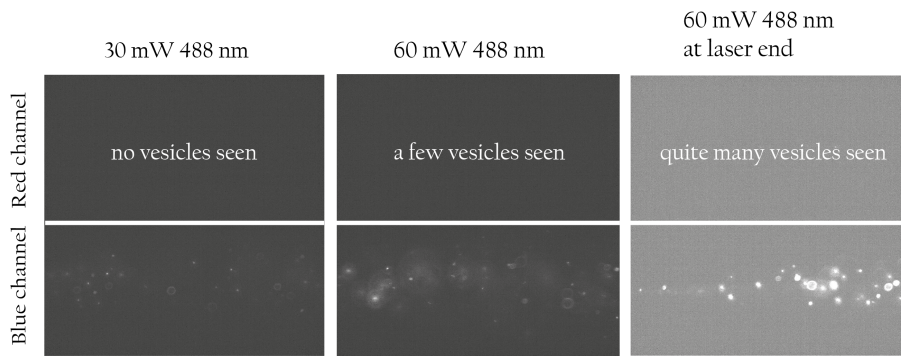


**Figure 6.5:** *Test of bleed-through in red channel from blue vesicles excited by blue laser. The upper part of each subimage corresponds to the red channel and the lower to the blue channel. Almost no vesicles were seen in the red channel, except when looking at an area directly at the edge of the laser fibre. As long as this area is avoided, the bleed-through is essentially negligible at these intensities.*

Both bleed-through and cross-talk could potentially complicate the colocalization analysis, and a range of laser intensities were tested to make sure there would not be trouble with bleed-through or cross-talk during measurements. A higher laser intensity would excite more fluorophores which increases the possibility of some emitting light that could be detected in the other channel. On the other hand as many fluorophore as possible should be excited to achieve many bright vesicles.

For testing the amount of bleed-through a sample of only one type of vesicles at a time was excited by the corresponding laser, i.e. blue vesicles were excited by blue laser and red vesicles excited by red laser. The experiments were performed with the colocalization setup for several laser intensities. The recorded movies from these experiments were examined manually looking for bleed-through events.

Snapshots from measurement with different laser intensities of the blue laser is shown in Figure 6.5. Each snapshot shows both the red and the blue channel, separated by a black line. The upper part corresponds to the  $700 \pm 38$  nm filter, i.e the red channel. The lower part corresponds to the blue channel ( $535 \pm 25$  nm). A few vesicles were seen in the red channel only when using a very high intensity (60 mW). As long as a lower intensity was used bleed-through was not a problem. In the same way, the red vesicles and red laser were investigated, resulting in a small amount of bleed-through at a very high intensity of 38 mV. Due to different softwares, the intensities of red and blue laser are measured in different units and it is thus difficult to compare these intensities quantitatively. It should also be noted that the scale of the red laser is inverted, so that 1 mV is a extremely high intensity, whereas 4000 mV is a low intensity.

To determine the amount of cross-talk a sample of blue vesicles was excited with red laser and vice versa. Snapshots from these measurements are shown in Figure 6.6 for very high laser intensities. Even at very high laser intensities, very few vesicles are noticeable.

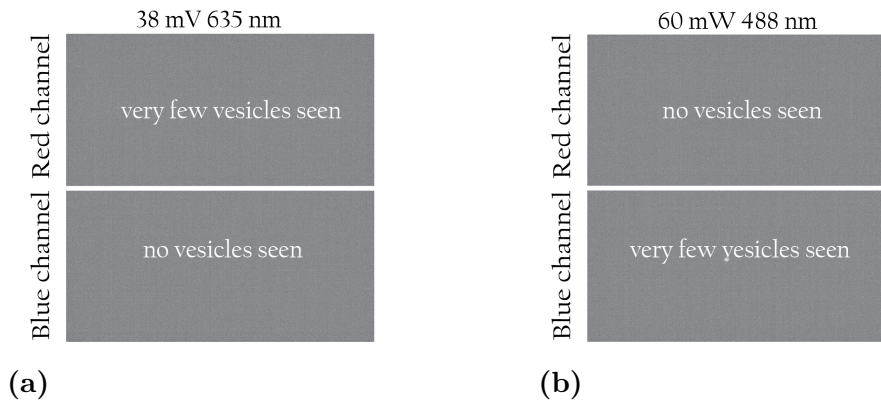


**Figure 6.6:** Examination of amount of crosstalk. In a), very few blue vesicles are excited by red laser even for extremely high intensities. In b), very few red vesicles are excited by blue laser at very high intensities.

The amount of bleed-through and cross-talk is thus very low, which was expected since the emission peaks in the spectra of the fluorophores being clearly separated, as was seen in Figure 6.4.

### 6.4.2 Limit of detection

A series of experiments were performed in order to determine the detection range for the colocalization assay. The experiment setup parameters were: red laser intensity 2061 mV, blue laser intensity 2 mW, exposure time 33 ms, number of frames per movie 1000.

As preparation for a measurement, 30  $\mu\text{l}$  of 10 pM red vesicles and 30  $\mu\text{l}$  10 pM blue vesicles were mixed with 30  $\mu\text{l}$  of a solution with different concentrations of SV40 VLPs dissolved in PBS. For negative control experiments, the SV40 solution was replaced with PBS buffer. This was incubated for 30 minutes and then separated into three subsamples. Each subsample was diluted 10 times with PBS buffer and put into the sample holder for measurement. The total vesicle concentration during a measurement was thus approximately 0.7 pM. The reason to dividing each sample into three subsamples was that initial measurements revealed a large variation between subsamples, and taking several measurements should result in a more reliable value of the amount of colocalization.

In Figure 6.7 a snapshot from an experiment with incubation with 300 pM VLPs is shown. This movie was examined manually by eye to get a first indication of the extent of colocalization. In Figure 6.7, potential colocalization events are marked with white circles. Each circle in the upper half of the figure has a counterpart in the lower half of the figure. For this concentration of VLPs, the amount of colocalization seems to be very high.

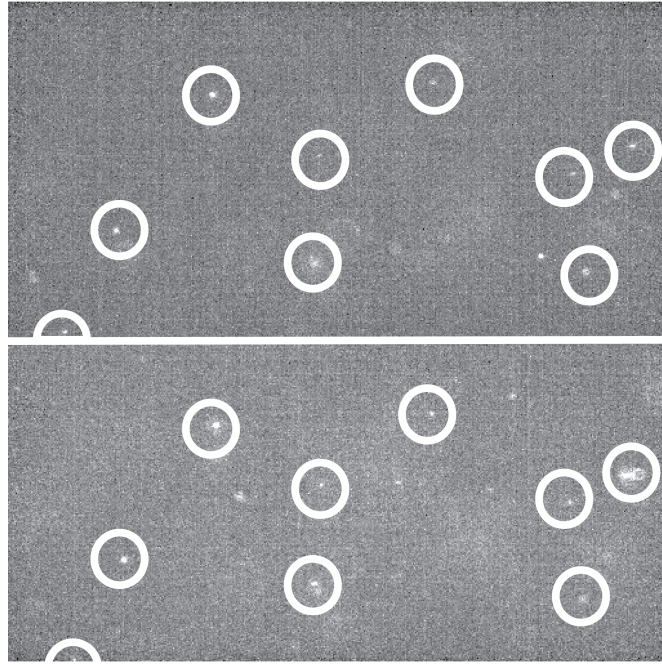


**Figure 6.7:** A snapshot from a positive control ( $[VLP] = 300 \text{ pM}$ ) with potential colocalization events marked with circles in the red and the blue channel.

All measurements were analysed with the tracking method described in 5.5, yielding the colocalization frequency for different concentrations of SV40. In Figure 6.8, a summary of the results is shown, with the colocalization frequency for concentrations of SV40 spanning a range of six orders of magnitude, from 1 fM to 1 nM. The experiments were replicated three times at separate days. A sigmoid function was also fitted to the data, with the equation:

$$y = A + \frac{B}{1 + Ce^{-Dx}}, \quad (6.4)$$

where  $x$  is the concentration of VLPs and the constants are  $A = 2.0$ ,  $B = 6.1$ ,  $C = 18.1$  and  $D = 1.5$ . Low VLP concentrations resulted in no contrast compared to the negative control with no VLPs, but at approximately 10 pM the colocalization frequency increases rapidly. The maximum colocalization frequency that was achieved was approximately 8 %.

In an attempt to extend the curve and to see whether the colocalization frequency saturates two more data points,  $\log([VLP] \text{ (pM)}) = 3.5$  and 4 ( $[VLP] = 3 \text{ nM}$  and 10 nM, respectively), were tested. However, for these two data points the colocalization frequency dropped to  $3.9 \pm 0.3 \%$  and  $3.2 \pm 0.5 \%$ . These data points were not included in Figure 6.8, since they were not consistent with the other data points, indicating a radical change in the system. A possible reason to this may be that the virus concentration is so high that the virus covers the vesicles so that the possibility for two complexes to aggregate becomes much smaller. For example, consider two vesicles that could potentially aggregate becoming covered by VLPs. For a few

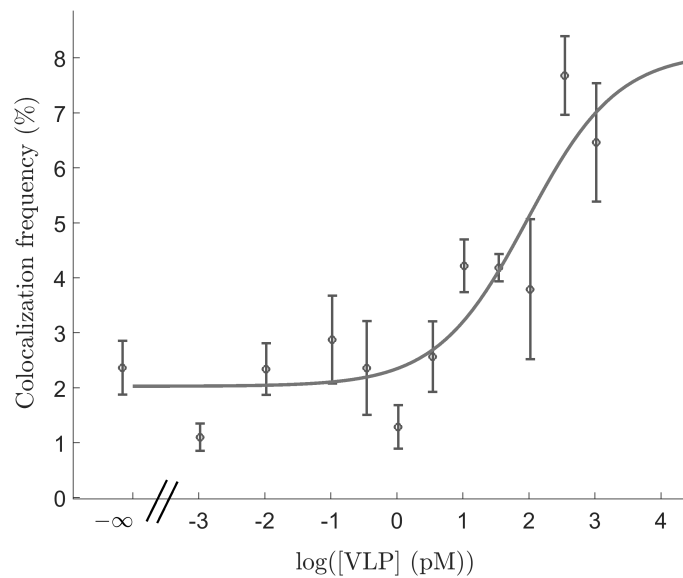


**Figure 6.8:** Colocalization frequency as a function of VLP concentration. The VLPs were incubated for 30 minutes with 10 pM red vesicles and 10 pM blue vesicles and diluted 10 times with PBS before measurement. The data is also fitted to a sigmoid function, of the form  $y = A + \frac{B}{1 + Ce^{-Dx}}$ .

VLPs attached to each vesicle, this induces a steric criterion for the occurrence of an aggregation. After a critical coverage, aggregation will become almost impossible if the VLPs do not attach to each other. This phenomenon is known to occur in some immunoassays and is called the *hook effect* [48].

Analysing a movie with this method took approximately one hour, meaning that the total time including incubation and measurement was approximately 1.5 hours.

#### 6.4.2.1 Dependence on incubation time

In the experiments resulting in Figure 6.8, the vesicles and VLPs were incubated for 30 minutes before measurement. The incubation time of 30 minutes was chosen because it was believed that this time should have resulted in enough collisions between vesicles and VLPs to have a significant effect. Some experiments were performed with different incubation times to investigate how this affected the colocalization frequency. The results from these measurements are shown in Figure 6.9. The error bars are large but it seems that a longer incubation time may result in a higher contrast, but the trade off is longer measurement times.

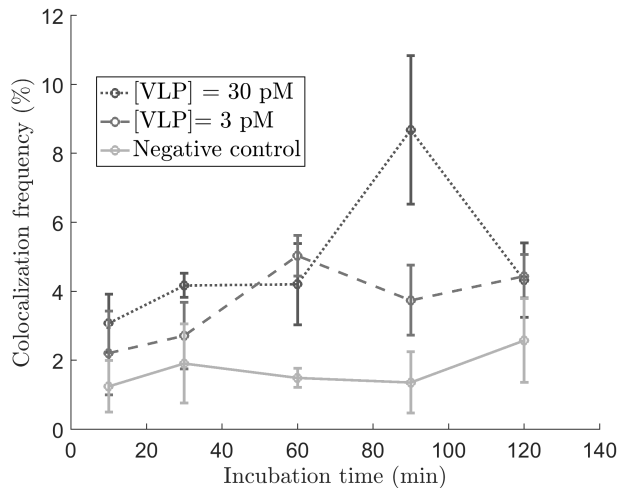


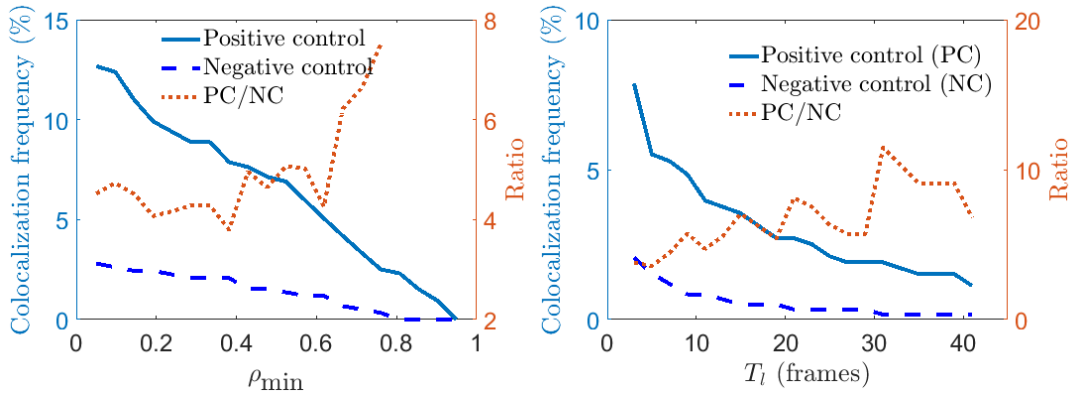
**Figure 6.9:** Colocalization frequency after different incubation time. The trend seems to be a higher contrast between negative control and measurements with VLPs after longer incubation times, but the error bars are large.

#### 6.4.2.2 Choice of analysis criteria

There were three parameters which could be tuned in the data analysis: the correlation criteria  $\rho_{\min}$ , i.e. how similar the tracks should be in order to be classified as colocalized, the track length criteria  $T_l$ , i.e. for how many frames the particle should be tracked in order to be analysed, and the position criteria,  $d_{\max}$ , i.e. how far the particles can be separated.

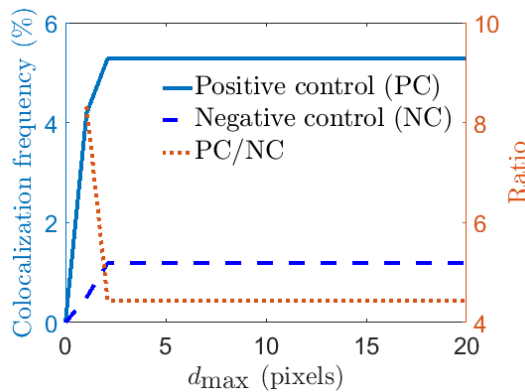
Tougher criteria would intuitively press down the number of colocalized events in both the negative and the positive control. A range of criteria was tested individually for a positive and a negative control in order to determine if there were any optimal criteria that yielded the largest contrast between the negative and the positive control. In Figure 6.10, the colocalization frequency for a positive control ([VLP]= 300 pM) and the colocalization frequency for a negative control is shown for different parameters. In each of the three subfigures, one parameter is varied with the two others held constant. When varying  $\rho_{\min}$  and  $T_l$ , the colocalization frequency decreases for stricter criteria, as would be expected. However, there is no clear maximum for the ratio between the positive and the negative control, even if the trend seems to be that tough criteria yield higher ratio. The position criterion did not affect the results, except at very small values. This is not surprising, since two colocalized vesicles are unlikely to be far away.

According to these figures, high values for  $\rho_{\min}$  and  $T_l$  yields higher ratios between these two samples, as the colocalization frequency in the control experiments gets closer to zero. However, as can also be seen, this presses down the range of the colocalization frequency. Since a clear maximum was not found, the parameters was chosen to be  $\rho_{\min} = 0.4$ ,  $T_l = 10$  and  $d_{\max} = 10$ , and used to calculate the colocalization frequency for Figure 6.8 in the previous section.



(a) Colocalization frequency for a positive control and a negative control for different values of  $\rho_{\min}$ .  $T_l$  and  $d_{\max}$  were held constant (7 and 10, respectively.)

(b) Colocalization frequency for a positive control and a negative control for different values of the track length.  $d_{\max}$  and  $\rho_{\min}$  were held constant (10 and 0.4, respectively).



(c) Colocalization frequency for a positive control and a negative control for different values of  $d_{\max}$ .  $T_l$  and  $\rho_{\min}$  were held constant (7 and 0.4, respectively).

**Figure 6.10:** Colocalization frequency for variation of one criteria while the other two were held constant.

### 6.4.2.3 Alternative analysis

An alternative analysis method was implemented to reduce the processing time. The alternative method was based on overlaying the channels in each frame, taking the aberration correction into account and by thresholding find overlaid vesicles, which would be counted as colocalized.

For each frame in a movie the image was separated into the red channel and the blue channel and background corrected separately, to account for any intensity differences between the two channels. Applying a low pass filter to the whole image then reduced the noise. Next a first threshold was applied to separate vesicles from the background. Pixel values below the threshold was set to 1, and pixel values above the threshold kept its original values.

In the next step each pixel in the red channel was multiplied with the corresponding pixel in the blue channel, using the aberration calculated in the colocalization method (see section 5.5.1). The idea in this step was that a pixel that did not belong to a vesicle in the red or the blue channel would become 1, a pixel that belonged to a vesicle in one channel, i.e. a non-colocalized vesicle would become around 30, whereas a pixel belonging to a vesicle in both the red and the blue channel would become around 900. By applying two thresholds, a high and a low, would give three categories of pixels: background, one vesicle or two overlaid vesicles. This enabled counting the ratio between colocalized vesicles and single vesicles for each frame in a movie, resulting in a mean colocalization frequency.

This algorithm was applied to the same movies as earlier, yielding the result in Figure 6.11. The data is also fitted to a sigmoid function of the form

$$A + \frac{B}{1 + Ce^{-Dx}}, \quad (6.5)$$

where  $A = 4.0$ ,  $B = 18.6$ ,  $C = 56.3$  and  $D = 2.3$ . Comparing to Figure 6.8, the increase of colocalization frequency occur at roughly the same concentration of VLPs as with the tracking analysis method.

In this method there is no need for tracking the vesicles, or determining the position with high resolution. It is thus much faster, if the aberration function is known. Then it takes approximately 100 seconds for a movie of 1000 frames to be analysed, compared to an hour for the tracking analysis. However, there is a larger possibility to detect false colocalization events because the vesicles in the two channels only have to be in the same place. This could be the reason to the colocalization frequency being consistently higher compared to Figure 6.8

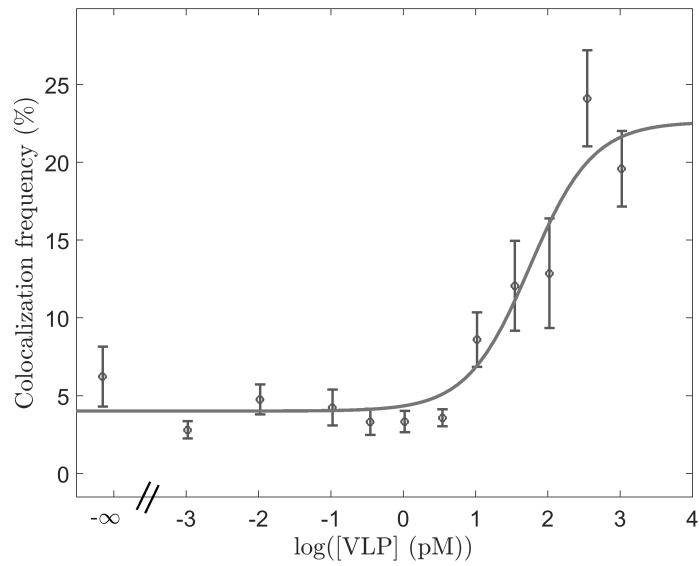


**Figure 6.11:** Colocalization frequency as a function of VLP concentration, fitted to a sigmoid function of the form  $A + \frac{B}{1+Ce^{-Dx}}$ .



# 7

## Discussion

**E**XPERIMENTS CAN RESULT in both expected and non-expected outcomes, and trying to understand the reasons to the achieved results is an important part of a project. In this chapter the experimental results are discussed further and some possible limitations in the setup and data analysis are brought up.

### 7.1 Limitations in colocalization assay

In section 4.3, the maximum colocalization frequency was discussed briefly, together with a theoretical estimation of the dynamic range. When scrutinizing the results in the previous sections, two main things can be noticed: the maximum colocalization frequency is far from the expected one and the amount of colocalization events in the negative control experiments is relatively high. The maximum colocalization frequency was expected to reach 100 % for very high concentrations of SV40, but it only reaches 8 %. This means that the contrast between the negative and positive control is only of the order of ten and this a surprising outcome. In the following sections, some possible reasons for these behaviours are discussed, including the appearance of unspecific interactions and limitations in the data analysis. Factors that could have a small effect on the result include for example that the concentration of blue and red vesicles are not equal due to human errors in the fabrication and while pipetting. It was also noticed during experiments that the focus planes are not identical, which could indicate that the red and the blue laser do not have an identical illumination profile.

One way to lower the limit of detection could be to use a lower concentration of vesicles, since a lower vesicle concentration would possibly lead to fewer free vesicles, as was discussed in section 4.3. But this would probably be at the cost of longer incubation times, since the collision frequency would decrease.

#### 7.1.1 Upper limit of virus concentration

As was mentioned in section 6.4.2, when adding 3 nM and 10 nM VLPs to the vesicles, this resulted in *less* colocalization, instead of the formation of few, very

large complexes as was expected beforehand. One possible reason is that at a critical VLP concentration, the system changes behaviour. Instead of the VLPs causing the forming of more and larger complexes, *fewer* complexes are formed. This leads to the idea that VLPs have two effects on the sample with vesicles. On one hand, the VLPs induces aggregation by acting as bridges between vesicles. On the other hand, VLPs also prevent aggregation by covering vesicles so that they cannot aggregate. Both these effects are possibly appearing at all concentrations, but for low concentrations, the first effect is dominating and for high concentration the second one dominates. However, to confirm this hypothesis, the behaviour at high virus concentrations should be investigated further.

## 7.1.2 Interrupted tracks

A potential problem in the data analysis is the interruption of tracks, i.e. one vesicle being counted two (or more) times due to the vesicle being "lost" for a couple of frames and then tracked again. This results in an exaggeration of the number of vesicles.

To which extent this problem appears is not known and there are several potential ways of trying to minimize this. One way could be to try to stitch together tracks that appears to belong to the same vesicle, for example two tracks in the same place, separated in time by only a few frames. However, the problem is then to define when two tracks belong to the same vesicle and when they do not. For example, for how many frames can the vesicle disappear, and how far is it allowed to displace?

Another possibility is to try to increase the time when the vesicles are in focus by making adjustments to the optical pathway in the setup. This was done briefly in this thesis by modifying the setup and performing a couple of experiments, which will be discussed in the section below.

### 7.1.2.1 Setup modification

In order to increase the depth of field, a 10 X objective was mounted on top the beamsplitter, and the 63 X objective was replaced with a 20 X air objective, resulting in a total magnification of 200 compared to the original magnification of 63. An illustration of the modified setup is shown in Figure 7.1. When examining the data manually, the vesicles seem to be in focus longer, but this is not reflected in the distribution of the length of detected tracks, presented in Figure 7.2. No significant difference between the two setups could be distinguished. A potential reason to this could be a decreased contrast between vesicles and background, leading to difficulties to track vesicles, breaking down a potentially long track into several short tracks. Another problem with this setup was that it was very difficult to find the focus plane when setting up the measurement. Yet another possibility is to use a water

immersion objective, since the ability of collecting light is better for water immersion objectives, thus the contrast between particles and background should be improved.

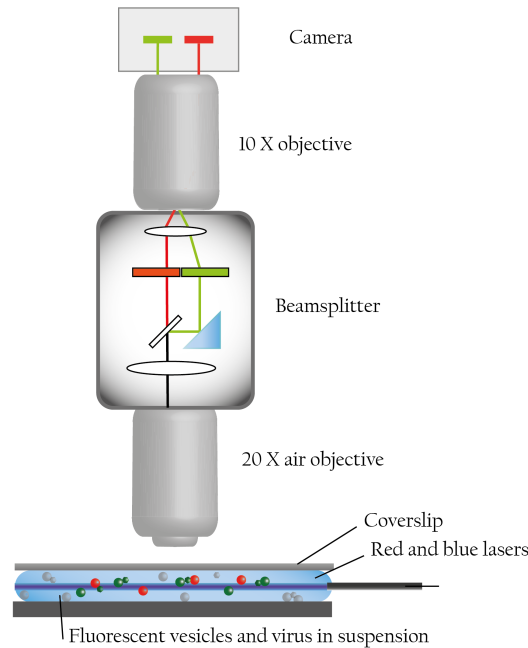


**Figure 7.1:** *Illustration of the modified setup, to be compared with Figure 5.3. An extra objective is mounted on top of the beamsplitter and the 63 X water immersion objective is replaced with a 20 X air objective.*

### 7.1.3 Unspecific interactions

The colocalization frequency for the control experiments was higher than expected, since vesicles were not initially believed to interact with each other. The results suggest that vesicles are interacting unspecifically and inducing colocalization events.

Comparing tracks from colocalization events in negative control and positive control experiments led to the conclusion that in most cases they could not be distinguished from each other. An example of this is shown in Figure 7.3, where an arbitrary colocalization event from a negative control is shown side by side with a colocalization event from a positive control. When investigating the distribution of the correlation measure  $\rho$ , no significant difference in the distribution was found between the events classified as colocalized in a negative control and a positive control. This is illustrated in Figure 7.4, where the distribution of the  $\rho_x$  values for events classified as colocalized in a negative control and a positive control. The distributions of  $\rho_y$  showed the same behaviour. This supports the claim that true colocalization events appear in the control experiments, with vesicles interacting unspecifically with each other. This is unwanted in this assay since it lowers the contrast between positive and negative control and increases the limit of detection.

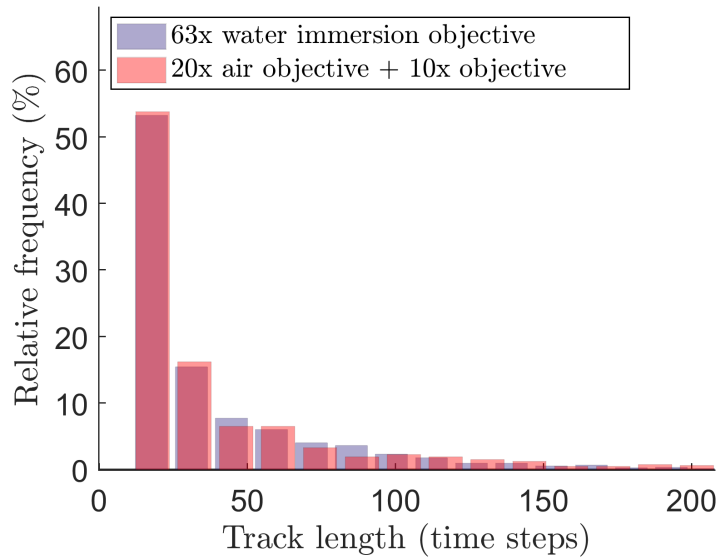


**Figure 7.2:** Track length (in time frames) for using an extra 10x objective in combination with 20x air objective, compared to track length for using 63x water immersion objective. No significant difference in terms of track length between the setups could be deduced.

Another possibility is the case of a vesicle in the blue channel being excited by the red laser and thus being seen in both channels, appearing as a colocalized complex. As was discussed in section 6.4.1, the laser intensities were chosen to avoid this problem, but occasionally having a vesicle behaving this way is not impossible.

#### 7.1.4 Problem with out-of-focus vesicles

One problem with the data analysis turned out to be vesicles that are not in focus and thus appear as large diffuse vesicles. In the detection analysis they were randomly detected; sometimes as one vesicle, sometimes as several. An example is shown in figure 7.5 where a diffuse out-of-focus vesicle was detected as 3 vesicles. This means that the total number of vesicles detected in a movie could be exaggerated, leading to a lower colocalization frequency. The problem is to distinguish between an out-of-focus vesicle and an in-focus vesicle. This could possibly be done by examining the intensity profile of a vesicle, since an out-of-focus vesicle has its highest intensity at the edges, whereas an in-focus vesicle is brightest in the centre. However, to do this for every detected vesicle is not trivial and would most likely require a lot of computations and was not implemented.

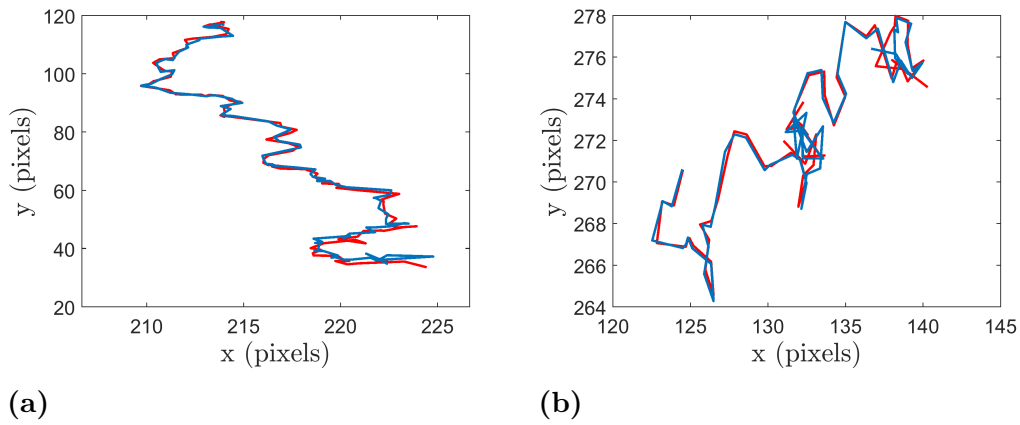


**Figure 7.3:** A randomly chosen colocalization event from a negative control (a) and a positive control (b). The red and blue lines corresponds to the overlaid tracks of the red and the blue particle, respectively. No significant differences between colocalization events in negative control compared to positive control could be deduced.

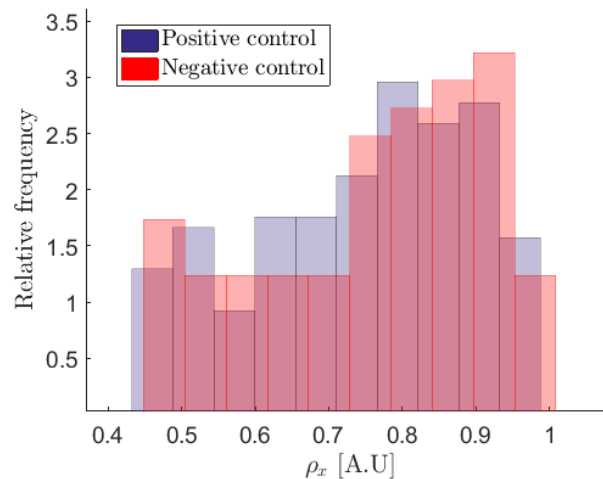


**Figure 7.4:** Distribution of correlation coefficient,  $\rho_x$  for negative control (red) and for positive control (blue). There is not a significant difference between the two distributions. Mean for positive controls: 0.71 with standard deviation 0.15, mean for negative controls: 0.73, standard deviation 0.16.

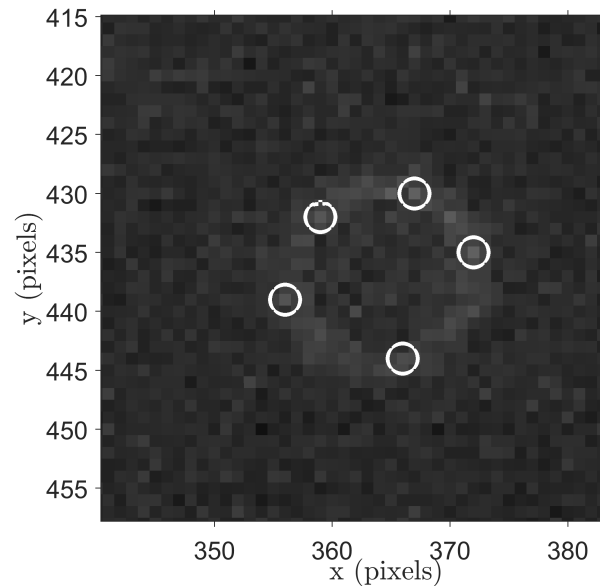


**Figure 7.5:** *An example of out-of-focus vesicle detected as several vesicles on the edge of the diffuse vesicle. The white circles mark detected vesicles in a certain time frame.*

## 7.2 Comparison between NTA and colocalization assay

Since the colocalization assay is in some senses a home-built variant of a commercial NTA device, it is natural to compare the two in terms of limit of detection. In both variants the particles are tracked individually, but in the commercial NTA the result is a size distribution, whereas in the colocalization assay individual events are identified. On beforehand, the colocalization assay was thought to have a lower limit of detection since individual events are counted instead of an ensemble. Even if one in the NTA gets the radius for individual particles, one can not distinguished between a large vesicle and a complex formed by several smaller. However, for NTA, the results indicate that a contrast between 1 pM and the control experiments could be seen, which is slightly better than the colocalization assay, where the limit of detection seems to be a couple of pM.

# 8

## Conclusion

THE AIM OF THIS WORK was to investigate a virus detection method based on fluorescence microscopy and particle tracking. In this chapter the main findings regarding the experimental work and setup are summarized.

With the current setup, the lowest concentration to be distinguished from the control was in the range of 10 pM. This could be done both with a colocalization/tracking method, and with a method based on overlaying the channels and simply counting vesicles. Measurements on the same sample had large variances and averaging the results from several measurements was necessary for reliable results. The samples were incubated for 30 minutes, and with a longer incubation time the limit of detection could probably be lowered, with the cost of a longer measurement time. A comparison between the experimental results and the estimations of the theoretical dynamic range shows that modelling the system as forming complexes with two vesicles and one virus-like particle is an oversimplification, and that larger complexes form to a great extent.

The number of colocalization events for the control experiments was not as low as expected, and the contrast between the maximum response and minimum response was on the order of ten. The colocalization events in the control experiments are probably due to unspecific interactions between vesicles, and this problem has to be addressed in order to lower the limit of detection.

One of the aims was to investigate if this method would be a potential candidate for a virus detector at an airport. For this being possible, the time scale for a measurement including data analysis should be one hour or less. The total time for performing a measurement was approximately 1.5 hours, compared to the one hour limit for using at an airport. The samples were incubated for 30 minutes, the measurement took approximately five minutes and the data analysis approximately 1 hour, depending on the vesicle concentration in the sample. With a faster computer the processing time could be reduced. The data analysis method was based on tracking particles and finding particles with correlated tracks. Using a simpler alternative data analysis method based on overlaying images and counting vesicles, the processing time was lowered to just a minute, resulting in a total measurement time of approximately 40 minutes, approximately with the same limit of detection.



# 9

## Future outlook

THE RESULTS in this thesis suggest that the colocalization assay works for the combination of SV40 VLPs and fluorescently labelled vesicles, even if the limit of detection was not very low. However, there are several ways of both testing the system further and improving the setup.

The amount of colocalization events in the negative controls was surprisingly high and a way to decrease the amount of colocalization for the negative control could be to stabilize the vesicles with for example PEG, a polymer often used to hinder aggregation of nanoparticles [49]. This could potentially decrease the background levels of colocalization. Of course it is necessary to test that the affinity between SV40 and GM1 is not affected by adding PEG to the vesicles. This could possibly be done by using QCM-D, as was used for testing the interaction between SV40 and vesicles. If the colocalization frequency could be lowered, this could lead to a lower limit of detection.

As was mentioned in an earlier chapter, the combination of objectives could also be modified in order to increase the depth of field to get the vesicles to stay in focus longer. In this thesis this was tested by adding an extra 10x objective, which seemed to get the vesicles in focus longer. However, this decreased the contrast so that the vesicles were harder to track. This resulted in tracks that were not longer than with the original setup. However, this was only tested briefly, and additional tests with for example water immersion objectives should be interesting to perform.

One other problem during experiments was the drift of particles due to flow. Drift of the particles could emerge as a result of an imbalance of the surface energy between the inlet and the outlet and the drift was hard to control. Therefore, a closed chamber could be an advantage, maybe in combination with a pump for controlling the flow. A small flow could be advantageous since more particles move through the field-of-view, whereas a large flow disturbs the measurements.

Furthermore, it would be interesting to use the same setup for testing another virus. For example, the norovirus could be suitable for further experiments, since it also binds to glycolipids, so that only small adjustments of the vesicles would be required [30]. The norovirus is more relevant for a real virus detection method, since SV40 does not target humans primarily.



# Bibliography

- [1] McNeill, W. H. *Patterns of disease emergence in history* (Oxford University Press, New York, 1993).
- [2] Black, F. L. Infectious diseases in primitive societies. *Science* **187**, 515–518 (1975).
- [3] Diamonds, J. *Vete, vapen, virus* (Norstedts, 2006).
- [4] Carrat, F. *et al.* Time lines of infection and disease in human influenza: a review of volunteer challenge studies. *American journal of epidemiology* **167**, 775–785 (2008).
- [5] Lessler, J. *et al.* Incubation periods of acute respiratory viral infections: a systematic review. *The Lancet infectious diseases* **9**, 291–300 (2009).
- [6] Corsica, F. Zika virus transmission from French Polynesia to Brazil (2015).
- [7] Sikka, V. *et al.* The emergence of zika virus as a global health security threat: A review and a consensus statement of the INDUSEM Joint working Group (JWG). *Journal of Global Infectious Diseases* **8**, 3 (2016).
- [8] Phillips, R., Kondev, J., Therlot, J. & Garcia, H. *Physical biology of the cell* (Garland Science, 2013), 2 edn.
- [9] Avanti Polar Lipids, Inc. 16:0-18:1 PC 1-palmitoyl-2-oleoyl-sn-glycero-3-phosphocholine 850457. URL [http://www.avantilipids.com/index.php?option=com\\_content&view=article&id=243&Itemid=208&catnumber=850457](http://www.avantilipids.com/index.php?option=com_content&view=article&id=243&Itemid=208&catnumber=850457). Accessed: 2016-02-22.
- [10] Reimhult, E., Zäch, M., Höök, F. & Kasemo, B. A multitechnique study of liposome adsorption on Au and lipid bilayer formation on SiO<sub>2</sub>. *Langmuir* **22**, 3313–3319 (2006).
- [11] Cann, A. J. *Principles of Molecular Virology (Standard Edition)* (Academic Press, 2005), 4 edn.
- [12] Lawrence, C. M. *et al.* Structural and functional studies of archaeal viruses.

- The Journal of biological chemistry* **284**, 12599–603 (2009).
- [13] Vilchez, R. A. & Butel, J. S. Emergent human pathogen simian virus 40 and its role in cancer. *Clinical microbiology reviews* **17**, 495–508 (2004).
- [14] Martini, F. *et al.* Simian virus 40 in humans. *Infectious agents and cancer* **2**, 13 (2007).
- [15] Ewers, H. *et al.* GM1 structure determines SV40-induced membrane invagination and infection. *Nature cell biology* **12**, 11–8; sup pp 1–12 (2010).
- [16] Neu, U., Woellner, K., Gauglitz, G. & Stehle, T. Structural basis of GM1 ganglioside recognition by simian virus 40. *Proceedings of the National Academy of Sciences of the United States of America* **105**, 5219–24 (2008).
- [17] Tsai, B. *et al.* Gangliosides are receptors for murine polyoma virus and SV40. *The EMBO journal* **22**, 4346–55 (2003).
- [18] Symian virus. URL [https://commons.wikimedia.org/wiki/File:Symian\\_virus.png](https://commons.wikimedia.org/wiki/File:Symian_virus.png). Accessed: 2016-05-26.
- [19] Santi, L., Huang, Z. & Mason, H. Virus-like particles production in green plants. *Methods (San Diego, Calif.)* **40**, 66–76 (2006).
- [20] Mocchetti, I. Exogenous gangliosides, neuronal plasticity and repair, and the neurotrophins. *Cellular and molecular life sciences : CMLS* **62**, 2283–94 (2005).
- [21] Bharati, K. & Ganguly, N. K. Cholera toxin: a paradigm of a multifunctional protein. *The Indian journal of medical research* **133**, 179–87 (2011).
- [22] Aman, A. T. *et al.* A mutant cholera toxin B subunit that binds GM1- ganglioside but lacks immunomodulatory or toxic activity. *Proceedings of the National Academy of Sciences of the United States of America* **98**, 8536–41 (2001).
- [23] Matrosovich, M., Matrosovich, T., Garten, W. & Klenk, H.-D. New low-viscosity overlay medium for viral plaque assays. *Virology journal* **3**, 1 (2006).
- [24] Goldman, E. Plaque assay for bacteriophage. In Goldman, E. & Green, L. H. (eds.) *Practical handbook of microbiology*, chap. 2 (CRC Press, 2015).
- [25] Cooper, P. The plaque assay of animal viruses. *Advances in virus research* **8**, 319 (1961).
- [26] Goldsmith, C. S. & Miller, S. E. Modern uses of electron microscopy for detection of viruses. *Clinical Microbiology Reviews* **22**, 552–563 (2009).
- [27] Jartti, T., Söderlund-Venermo, M., Hedman, K., Ruuskanen, O. & Mäkelä, M. J. New molecular virus detection methods and their clinical value in lower respiratory tract infections in children. *Paediatric respiratory reviews* **14**, 38–45

- (2013).
- [28] Welzel, T. M. *et al.* Real-time PCR assay for detection and quantification of hepatitis B virus genotypes A to G. *Journal of clinical microbiology* **44**, 3325–33 (2006).
- [29] Rabenau, H. *et al.* Laboratory diagnosis of norovirus: which method is the best? *Intervirology* **46**, 232–238 (2003).
- [30] Bally, M., Graule, M., Parra, F., Larson, G. & Höök, F. A virus biosensor with single virus-particle sensitivity based on fluorescent vesicle labels and equilibrium fluctuation analysis. *Biointerphases* **8**, 4 (2013).
- [31] Gan, S. D. & Patel, K. R. Enzyme immunoassay and enzyme-linked immunosorbent assay. *Journal of Investigative Dermatology* **133**, 1–3 (2013).
- [32] Agrawal, A., Deo, R., Wang, G. D., Wang, M. D. & Nie, S. Nanometer-scale mapping and single-molecule detection with color-coded nanoparticle probes. *Proceedings of the National Academy of Sciences of the United States of America* **105**, 3298–303 (2008).
- [33] Ho, Y.-P., Kung, M. C., Yang, S. & Wang, T.-H. Multiplexed hybridization detection with multicolor colocalization of quantum dot nanoprobe. *Nano Letters* **5**, 1693–1697 (2005).
- [34] Han, Y., Alsayed, A., Nobili, M. & Yodh, A. G. Quasi-two-dimensional diffusion of single ellipsoids: Aspect ratio and confinement effects. *Physical Review E - Statistical, Nonlinear, and Soft Matter Physics* **80**, 1–6 (2009).
- [35] Bhaduri, B., Neild, A. & Ng, T. W. Directional Brownian diffusion dynamics with variable magnitudes. *Applied Physics Letters* **92**, 5–8 (2008).
- [36] ATTO-TEC. ATTO 488. URL [https://www.atto-tec.com/attotecshop/product\\_info.php?language=en&info=p99\\_ATTO-488.html](https://www.atto-tec.com/attotecshop/product_info.php?language=en&info=p99_ATTO-488.html). Accessed: 2016-03-09.
- [37] ATTO-TEC. ATTO 633. URL [https://www.atto-tec.com/attotecshop/product\\_info.php?info=p110\\_atto-633.html](https://www.atto-tec.com/attotecshop/product_info.php?info=p110_atto-633.html). Accessed: 2016-03-09.
- [38] Turner, G. K. An absolute spectrofluorometer a new instrument has been developed for simple determinations of absolute fluorescence spectra. *Science* **146**, 183–189 (1964).
- [39] Qsense. Quartz crystal microbalance with dissipation monitoring (QCM-D) . Technology note. URL [http://www.biolinscientific.com/zafepress.php?url=/pdf/Q-Sense/Technology%20Notes/QS\\_TN\\_qcm-d.pdf](http://www.biolinscientific.com/zafepress.php?url=/pdf/Q-Sense/Technology%20Notes/QS_TN_qcm-d.pdf). Accessed: 2016-04-07.
- [40] Frost, R. *et al.* Acoustic detection of melanosome transport in *Xenopus laevis*

- melanophores. *Analytical biochemistry* **435**, 10–8 (2013).
- [41] Edvardsson, M. *QCM-D- with focus on variations in oscillation amplitude*. Ph.D. thesis, Chalmers University of Technology, Göteborg, Sweden (2006).
- [42] Granéli, A., Rydström, J., Kasemo, B. & Höök, F. Formation of supported lipid bilayer membranes on SiO<sub>2</sub> from proteoliposomes containing transmembrane proteins. *Langmuir* **19**, 842–850 (2003).
- [43] Malvern Technologies. High resolution sizing and concentration measurements of sub-visible protein aggregates using NTA. Technical note (2015).
- [44] Malvern Technologies. Fluorescence nanoparticle detection using NTA. Technical note (2015).
- [45] Filipe, V., Hawe, A. & Jiskoot, W. Critical evaluation of Nanoparticle Tracking Analysis (NTA) by NanoSight for the measurement of nanoparticles and protein aggregates. *Pharmaceutical research* **27**, 796–810 (2010).
- [46] Rice, J. *Mathematical statistics and data analysis* (Nelson Education, 2006).
- [47] Ruprecht, V., Weghuber, J., Wieser, S. & Schütz, G. J. Measuring colocalization by dual color single molecule imaging: Thresholds, error rates, and sensitivity. In Iglic, A. & Kulkarni, C. V. (eds.) *Advances in Planar Lipid Bilayers and Liposomes*, chap. 2, 21–37 (Academic Press, 2014).
- [48] Tate, J. & Ward, G. Interferences in immunoassay. *Clinical Biochemist Reviews* **25**, 105–120 (2004).
- [49] Jones, R. A. *Soft Condensed Matter* (Oxford University Press, 2002).